Escola de Camins
Escola Tècnica Superior d'Enginyeria de Camins, Canals i Ports
UPC BARCELONATECH

TESINA D'ESPECIALITAT

Títol

DAMAGE INITIATION AND PROPAGATION IN NON-LOCAL GRADIENT MODELS BASED ON DISPLACEMENT SMOOTHING

Autor/a

MESTRE BELLIDO, HÉCTOR

Tutor/a

RODRÍGUEZ-FERRAN, ANTONIO

Departament

Departament d'Enginyeria Civil i Ambiental

Intensificació

Enginyeria Computacional

Data

Gener del 2016

Abstract

Damage initiation and propagation in non-local gradient models based on displacement smoothing

by Héctor Mestre Bellido

In the framework of damage models, non-local models based on displacement smoothing are known to have similar regularisation capabilities to standard models (based on equivalent strain smoothing).

The aim of this thesis is to evaluate how well these alternative models describe the damage initiation and damage propagation processes. To illustrate this, two critical problems are considered. Damage initiation is analysed by means of a specimen with a pre-existing crack under mode I failure, and shear band formation is used to discuss damage propagation.

In the past, standard models have been shown to incorrectly describe the damage initiation and damage propagation phenomena in these two problems. Standard models predicted damage initiation away from the the crack tip, and non-physical migration of the shear band during damage propagation.

The numerical results in this thesis show that the proposed alternative models correctly predict damage initiation at the crack tip, and correctly describe damage propagation, with no shear band migration.
To ensure realistic damage propagation, special care must be taken in the choice of two key material parameters: characteristic length ℓ and post-peak slope of the damage law β. Following this direction, the effect of ℓ and β in the the ductility and the shear band width has been studied and quantified.

The results from numerical experiments also hint at the possibility that standard models, with small adjustments, could be able to remove the shear band migration in damage propagation processes. For that purpose, analogous studies of ℓ and β should be carried out.

Resum

Damage initiation and propagation in non-local gradient models based on displacement smoothing

by Héctor Mestre Bellido

Dins el marc dels models de dany, els models no-locals basats en la regularització dels desplaçaments tenen una capacitat de regularització semblant a la dels models estàndards (basats en la regularització de la deformació equivalent).

L'objectiu d'aquesta tesina és evaluar com aquets models descriuen els fenòmens d'inici i propagació de dany. Amb aquest objectiu, s'analitzen dos problemes crítics.

L'inici de dany s'estudia en una proveta amb una pre-fisura i es somet a mode I de rotura, mentre que s'estudia la propagació de dany durant la formació d'una banda de tallant.

Prèviament s'ha demostrat que els models estàndards prediuen incorrectament l'inici de dany en un punt allunyat de la pre-fisura, i una migració de la banda de tall que contradiu els experiments físics a laboratori.

Els resultats d'aquesta tesina mostren que els models alternatius proposats son capaços de predir l'inici de dany a la pre-fisura, així com propagar el dany sense causar una migració de la banda de tall. Però per tal d'assegurar que tal migració no es produeix, els paràmetres materials longitud característica ℓ i pendent post-pic de la llei de dany β han d'escullir-se amb especial cura. Per aquest motiu, s'ha estudiat cuidadosament l'efecte d'aquests dos paràmetres en la banda de dany i en la ductilitat.

A més, els resultats numèrics semblen indicar que, amb petits ajustos els models estàndards podrien ser capacos d'eliminar la migració de la banda de dany. Realitzant anàlisis anàlogues a les anteriors, en aquest cas pels models estàndards, permetria confirmar-ho.

Acknowledgements

There are many people who have contributed directly or indirectly to this thesis.

My thesis advisor, Antonio Rodríguez-Ferran, deserves an special mention. Thanks for giving me the background in the topic of non-local models, discussing results and patiently answering every question I had. Thanks for encouraging me to go one step further, I am really happy with the ending result. Lastly, thanks for your "*Senyor Héctor Mestre, no pots fer això. És com si un jugador d'escacs...*" it made me realise how obvious a lot of things I always underestimated were.

I want to thank Elena Tamayo-Mas for sharing part of the code from her PhD, it was really useful as a baseline. I also want to thank all the people who researched the world of non-local models, and the scientific community in general.

Lastly, I want to thank my friends who helped me not to go crazy, you know I love you all!

And of course, my parents. Thanks for helping me to always focus on the positive side of things.

Contents

List of Figures

Chapter 1

Introduction

1.1 Goals and motivation

Material softening is one of the hot topics in engineering and material science. To understand the behaviour of softening materials, it is necessary to be able to reliably predict crack initiation and propagation. To this end, there are two possible approaches: experimental physical tests, and numerical simulations.

These approaches do not exclude each other, they are complementary. But numerical tests have one big advantage over physical ones: once a numerical model is built, new experiments can be executed at near zero cost. This allows to gather data at a fast speed, and to study a wider amount of conditions.

The subject of numerical models in the field of material softening has been deeply studied. One of the most popular approaches is damage mechanics, which is a branch of continuum mechanics. Initially, only classic local formulations were used, but by the end of the 20th century some problems of the local formulations became evident, and non-local models started to proliferate, as a cure to those problems [2].

However, non-local models are not exempt of his own limitations. The starting point of this master thesis is the research carried out in [1], which points out that non-local gradient enhanced standard models can fail to predict correct damage initiation and correct damage propagation. On the other hand, it has been suggested that models based on the smoothing of the displacement field keep the regularisation effects of standard models [3] [4]. From now on, we will refer to this last type of models as "alternative models".

The main goal of this thesis is to prove that alternative models do not share the same limitations that standard models have, and are able to correctly predict damage softening, in regards to both damage initiation and damage propagation. As alternative models are fairly new, other secondary goals are also assessed, such as the discussion of boundary conditions and numerical parameters, and the effect that singularities have in the model.

1.2 Damage models

As mentioned earlier, damage mechanics is a branch of continuum mechanics, at the same level of elasticity or plasticity. Damage models are defined by

$$\boldsymbol{\sigma} = \big(1 - D\big)\mathbf{C}\boldsymbol{\varepsilon} \qquad \text{Constitutive equation} \tag{1.1}$$

$$D = D(\kappa) \qquad \text{Damage parameter} \tag{1.2}$$

$$\kappa(t) = \max_{\tau \leq t} e(\tau) \qquad \text{History variable} \tag{1.3}$$

where $\boldsymbol{\sigma}$ is the stress, $\mathbf{C}$ is the four-order stiffness tensor, $\boldsymbol{\varepsilon}$ is the strain, t is time and e is the equivalent strain (equations (1.8), (1.10) and (1.11)). D ranges between 1 (maximum damage) and 0 (undamaged specimen). The explicit formulation of equation (1.2) depends on the specifics of the damage model being used, as there are different alternatives.

Looking at equation (1.1) it can be observed that, if we removed the coefficient $(1 - D)$, we would have an elastic model. In other words, when damage is 0, damage model's behaviour is elastic.

Then, when the specimen gets damaged, D becomes bigger, so the coefficient $(1 - D)$, that multiplies the stiffness tensor, becomes smaller. In other words, when the specimen is being damaged, the softening is being modelled as a reduction of the stiffness.

A typical strain-stress curve from damage models is shown in figure 1.1.

1.3 Non-local models

Traditional models that study material softening are local. This means that the stress at a given point depends solely on the deformation at that given point. The only interaction

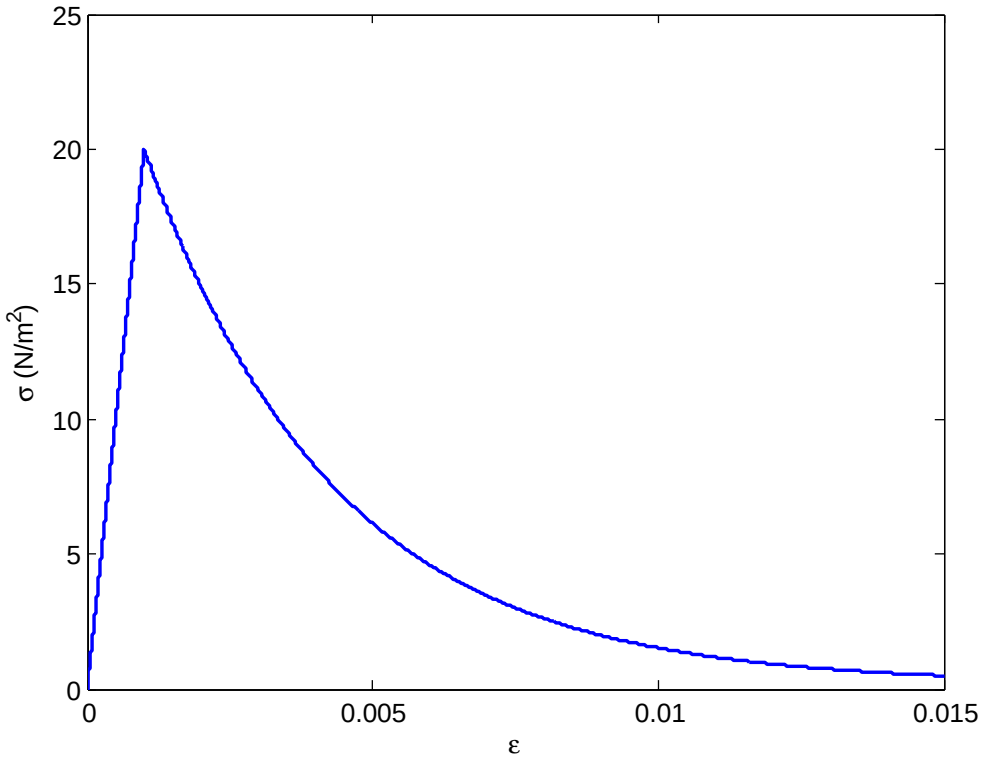

FIGURE 1.1: Typical strain-stress curve with damage models

between different points is by means of the balance equations (mass, momentum, energy and entropy) [2].

On the opposite, in non-local models, a certain variable is substituted by its non-local counterpart. This non-local variable at a given point does not depend only on the point itself, but also on its neighbourhood. The size of this neighbourhood is defined by a characteristic length ℓ, and it is related to the properties of the material at a small scale.

Non-local models have been proliferating during the last decades because they are able to overcome three basic limitations of the local models [2].

1. Inability to capture small deviations caused by material heterogeneity.
2. Inability to capture size effects.
3. Pathological mesh dependence. The boundary value problem is ill-posed, and local models have problems achieving convergence in the solutions.

There are two different formulations for non-local models: integral and gradient. Gradient formulations are more commonly used than integral ones, due to being easier to implement at the boundaries.

In integral formulations, the non-local variable is obtained by performing a weighted average of the local variable at the points in a neighbourhood [2] (the closer these points are to the given point, the more weight they have). Given a local variable $\boldsymbol{f}$, its non-local counterpart $\widetilde{\boldsymbol{f}}$ can be found as

$$\widetilde{\boldsymbol{f}}(\boldsymbol{x}) = \int_V \alpha(\boldsymbol{x}, \boldsymbol{\chi}) \boldsymbol{f}(\boldsymbol{\chi}) d\boldsymbol{\chi} \tag{1.4}$$

where α is the weighing function.

Gradient formulations express the same idea of non-locality, but with a gradient formulation instead of an integral one. This is done by solving the partial differential equation

$$\widetilde{\boldsymbol{f}}(\boldsymbol{x}) - \ell^2 \nabla^2 \widetilde{\boldsymbol{f}}(\boldsymbol{x}) = \boldsymbol{f}(\boldsymbol{x}) \tag{1.5}$$

1.4 Non-local gradient models: standard models

In standard models the regularised (non-local) variable is the equivalent strain e [5]. The differential equation to solve is

$$\widetilde{e}(\boldsymbol{x}) = -\ell^2 \nabla^2 \widetilde{e}(\boldsymbol{x}) = e(\boldsymbol{x}) \quad \text{in } \Omega \tag{1.6}$$

with boundary conditions

$$\nabla \widetilde{e} \cdot \boldsymbol{n} = 0 \qquad \text{on } \partial\Omega \tag{1.7}$$

There are different formulations of the equivalent strain e. In this thesis we use the most common ones: von Mises, modified von Mises and simplified Mazars [3].

Von Mises

$$e = \frac{1}{1+\nu}\sqrt{3J_2} \tag{1.8}$$

with ν the Poisson's ratio and J_2 the invariant of the strain tensor defined as

$$J_2 = \frac{1}{\mathrm{tr}(\boldsymbol{\varepsilon} \cdot \boldsymbol{\varepsilon}) - \frac{1}{3}\mathrm{tr}^2(\boldsymbol{\varepsilon})} \tag{1.9}$$

Modified von Mises, which includes the effect of the mean strain [6]

$$e = \frac{k-1}{2k(1-2\nu)} I_1 + \frac{1}{2k}\sqrt{\left(\frac{k-1}{1-2\nu} I_1\right)^2 + \frac{12k}{(1+\nu)^2} J_2} \tag{1.10}$$

with I_1 the first tensorial invariant of the strain tensor, and k the ratio of compressive strength to tensile strength.

Simplified Mazars [7]

$$e = \sqrt{\sum \widehat{\varepsilon_i}^2} \tag{1.11}$$

with ε_i the principal strains and $\widehat{\varepsilon_i}$ the positive principal strain:

$$\widehat{\varepsilon_i} = \frac{\varepsilon_i + |\varepsilon_i|}{2} \tag{1.12}$$

1.5 Non-local gradient models: alternative models

In alternative models, a different approach is taken, and that is smoothing the local displacement field $\boldsymbol{u}$. The differential equation to solve is

$$\widetilde{\boldsymbol{u}}(\boldsymbol{x}) = -\ell^2 \nabla^2 \widetilde{\boldsymbol{u}}(\boldsymbol{x}) = \boldsymbol{u}(\boldsymbol{x}) \tag{1.13}$$

and its boundary conditions will be extensively discussed in section 2.3.

Once the non-local displacement field $\widetilde{\boldsymbol{u}}$ is found, it can be used to compute the non-local strain tensor [8].

$$\widetilde{\boldsymbol{\varepsilon}} = \nabla^s \widetilde{\boldsymbol{u}} \tag{1.14}$$

where ∇^s is the symmetric gradient operator.

Afterwards, the non-local equivalent strain is found applying (1.8), (1.10) and (1.11) to the non-local strain $\widetilde{\boldsymbol{\varepsilon}}$.

Chapter 2

Damage initiation

2.1 Introduction

Regularised damage models are being used in order to overcome the well-known problems of local approaches, but these models also have some limitations. As pointed out in [1], standard models predict non-physical damage initiation away from the crack tip in mode I problems.

Throughout this chapter, traditional standard models will be compared with the proposed alternative models, in regards to damage initiation. The main purpose of the chapter is to prove that alternative models are better than standard ones, because they are able to correctly predict damage initiation at the crack tip.

The goals in this chapter are:

1. **To discuss the adequateness of different boundary conditions for the regularisation equation** (1.13). Different boundary conditions have been analysed in the past [3] [9]. We will verify that the conclusions in [3] are valid for the different numerical tests that will be carried out in this master thesis.

2. **To justify correct damage initiation**. Standard models fail to predict correct damage initiation at the crack tip [1]. We will justify that alternative models are better because they are able to reproduce correct damage initiation.

3. **To study the effect of singularities on the local displacement field**. Some physical problems may lead to singularities (i.e infinitum values at some points of

the strain and stress fields). We will study how these singularities affect each step of both standard strain based models and the proposed displacements method, and which are their consequences.

4. **To generalize the applicability of previous results to different mechanical conditions**. We want to ensure that the strengths of our proposed method are not related to a very specific combination of mechanical and numerical parameters. With this in mind, we do some more tests that emulate different physical conditions, and check that the points done on previous sections are still valid.

2.2 Description of the tests

2.2.1 Geometry

Damage initiation in mode I is analysed by means of the compact tension specimen with a pre-existing crack of length h = 0.5 mm, as shown in figure 2.1. Physical experiments reveal that the damage starts at the crack tip. The reasons why this case has been chosen are:

- The pre-existing crack ensures the specimen will follow mode I failure, and will start breaking at the crack tip.
- This is the case in which standard gradient models failed to predict damage initiation at the crack tip [1].

2.2.2 Analytical considerations

In this example we are studying damage initiation, and we do not care about damage propagation. Before damage initiation the behaviour of the material is purely elastic, so we can use theory of material elasticity to analyse the problem.

The elastic problem has already been solved [10], here we show the analytical expressions for displacements and strain fields at a distance r and angle θ from the crack tip (figure 2.2).

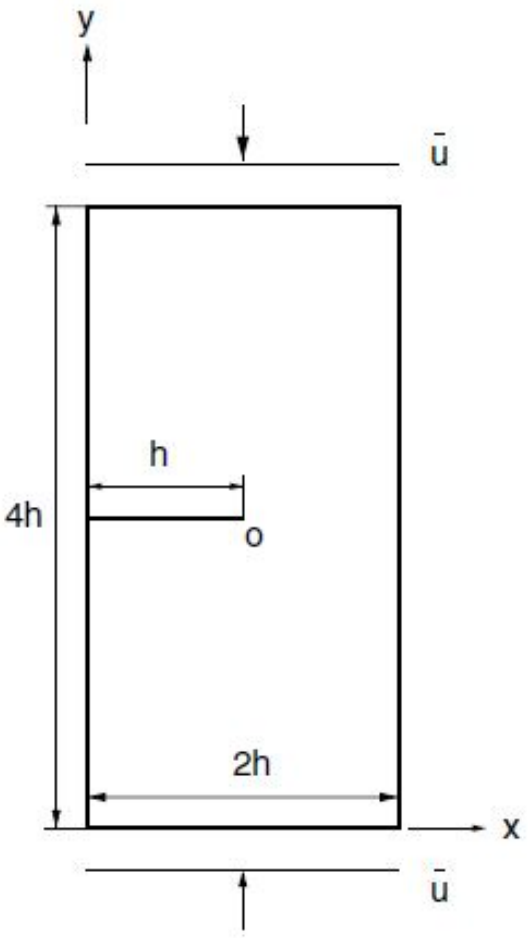

FIGURE 2.1: Geometry and loads of the specimen, from [1]

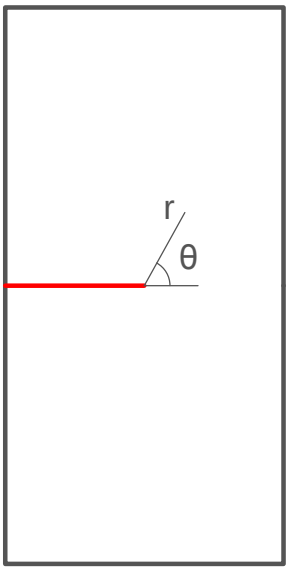

FIGURE 2.2: distance r and angle θ from the crack tip

$$u_x = (1+\nu)\frac{K_I}{2E\sqrt{2\pi}}\sqrt{r}\left[(2\kappa-1)\cos\frac{\theta}{2} - \cos\frac{3}{2\theta}\right] \tag{2.1}$$

$$u_y = (1+\nu)\frac{K_I}{2E\sqrt{2\pi}}\sqrt{r}\left[(2\kappa-1)\sin\frac{\theta}{2} - \sin\frac{3}{2\theta}\right] \tag{2.2}$$

with

$$\kappa = \frac{3-\nu}{1+\nu} \qquad \text{for plane stress} \tag{2.3}$$

$$\kappa = 3-4\nu \qquad \text{for plane strain} \tag{2.4}$$

$$\varepsilon_{xx}(r,\theta) = \frac{K_I}{E\sqrt{2\pi r}}\cos\frac{\theta}{2}\left[1-\sin\frac{\theta}{2}\sin\frac{3\theta}{2}\right] \tag{2.5}$$

$$\varepsilon_{yy}(r,\theta) = \frac{K_I}{E\sqrt{2\pi r}}\cos\frac{\theta}{2}\left[1+\sin\frac{\theta}{2}\sin\frac{3\theta}{2}\right] \tag{2.6}$$

$$\varepsilon_{xy}(r,\theta) = \frac{K_I}{E\sqrt{2\pi r}}(1+\nu)\cos\frac{1}{2}\theta\sin\frac{1}{2}\theta\cos\frac{3}{2}\theta \tag{2.7}$$

We can observe that strain fields become singular near the crack tip, when r tends to 0. On the other hand, displacement fields do not have such singularity, and in fact they are continuous along all the domain.

At this point the reader might be asking why are we worrying about the analytical expression of displacements and strains, when our model should be calculating them. We do that for a couple of different reasons:

- The local strains field have singularities at the crack tip, whereas local displacements do not. How singularities are treated in the models is a relevant fact and will be discussed extensively on section 2.5.
- When facing an unknown problem, two different sets of differential equations have to be solved: the ones corresponding to the mechanical problem and the ones corresponding to the regularisation equation (1.5).

  By means of the analytical expressions we can separate the mechanical problem (whose solution is known) from the regularisation problem. This has two major advantages:

  1. The problem becomes simpler and computationally faster to solve.

2. The mechanical equations do not interfere in the regularisation equations, so we can be sure that the behaviour observed from the tests only depends on the regularisation model.

2.2.3 Numerical considerations

All the calculations and figures shown in this thesis have been done using the software Matlab.

In the numerical simulations only the upper part of the specimen has been discretised due to symmetry, and the load has been applied via an imposed displacement.

Different meshes used in the numerical simulations are shown in figure 2.3. To avoid placing a node at the crack tip, the number of elements in each row has to be odd. The characteristic length is $\ell = 0.2$ mm.

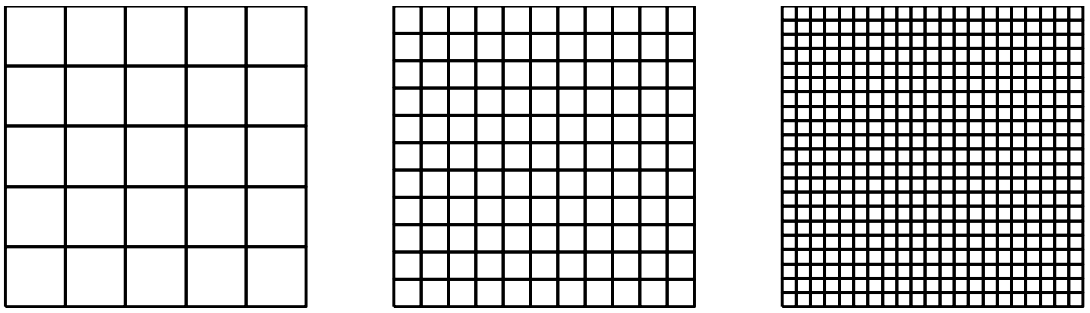

(A) 5×5 elements (B) 11×11 elements (C) 21×21 elements

FIGURE 2.3: Example of meshes used

The expressions of the strain and displacement fields are multiplied by a factor of $\frac{K_I}{2E\sqrt{2\pi}}$. As this is a constant that affects both the standard and alternative models, it does not provide useful information for comparison purposes, and is ignored as such.

2.3 Boundary conditions

The choice of adequate boundary conditions in the regularisation equation (1.5) is one of the first problems that arise from using alternative models. For standard models, homogeneous Neuman boundary conditions are used [3], but this does not mean that these boundary conditions are also suited for alternative models.

For starters, the equivalent strain e is scalar, whereas the displacement field $\mathbf{u}$ is a vector of two or three components (for 2D or 3D problems). Because of that, alternative models require a higher number of boundary conditions. This poses an added layer of complexity to alternative models, but at the same time offers more flexibility to adjust them to the behaviour observed in empirical experiments.

Previous research about this topic has already been carried out [3] [9]. The goodness of each type of boundary condition was evaluated according to the following four parameters:

1. Reproducibility of order 1 ($\boldsymbol{u}$ is linear $\Longrightarrow \widetilde{\boldsymbol{u}}$ is linear)
2. Displacement smoothing along the boundary
3. Local response normal to boundaries
4. Volume preservation

The boundary conditions considered were Dirichlet, homonegenous Neumann, non-homogeneus Neumann and combined boundary conditions. Combined boundary conditions are a mixture of the other ones. That is, to prescribe Dirichlet boundary conditions for the normal component of the displacement field and non-homogeneus Neumann boundary conditions for the tangential components:

$$\left.\begin{aligned} \widetilde{\boldsymbol{u}} \cdot \boldsymbol{n} &= \boldsymbol{u} \cdot \boldsymbol{n} \\ \nabla(\widetilde{\boldsymbol{u}} \cdot \boldsymbol{t}) \cdot \boldsymbol{n} &= \nabla(\boldsymbol{u} \cdot \boldsymbol{t}) \cdot \boldsymbol{n} \end{aligned}\right\} \text{ on } \partial\Omega \tag{2.8}$$

Figure 2.4 shows a summary of the results.

Because the use of adequate boundary conditions is the starting point in this thesis, it is vital that these results are correct. So, not only the previous results have been verified, but the boundary conditions have also been tested for the problem described in section 2.2. This is done in order to ensure that the singularities in displacement fields do not affect previous conclusions.

	Dirichlet	Homogeneous Neumann	Non-homogeneous Neumann	Combined
Reproducibility of order 1	✓	×	✓	✓
Displacement smoothing along the boundary	×	✓	✓	✓
Local response normal to boundaries	✓	×	×	✓
Volume preservation	✓	×	×	✓

FIGURE 2.4: Advantages of each boundary condition

Local and regularised displacement fields are shown in figures 2.5 and 2.6. As both fields are rather similar, both contour plots and three-dimensional representations are shown. We can observe than combined boundary conditions allow for displacement smoothing while maintaining a local response normal to boundaries, so these boundary conditions will be used in all future calculations in this thesis.

2.4 Non-local equivalent strain profiles

The non-local equivalent strain is one of the most important variables in the model, as it is the driving factor that determines the damage. In other words, damage only depends on the non-local equivalent strain and the shape of the damage evolution law.

Different damage laws can be used, but in all of them the higher the equivalent strain, the higher the damage, as it will be shown in equations (3.1) and (3.5). For that reason, as surprising as it might sound, focusing on non-local equivalent strain instead of damage is better, because this separates the shape of the damage law from the calculation of the driving factor.

Contour plots of the non-local equivalent strain at damage initiation are reported in figure 2.7.

In regards to the standard model, we verify the conclusions in [1]: the maximum of the non-local equivalent strain has shifted to the right, so the damage is predicted to start away from the crack tip. Incorrect damage initiation is also reported in case of cracks or notches modelled as strongly non-convex entities with non-zero volume, i.e. when there are no strain singularities. Non-constant characteristic length was proposed as a cure to this problem [1].

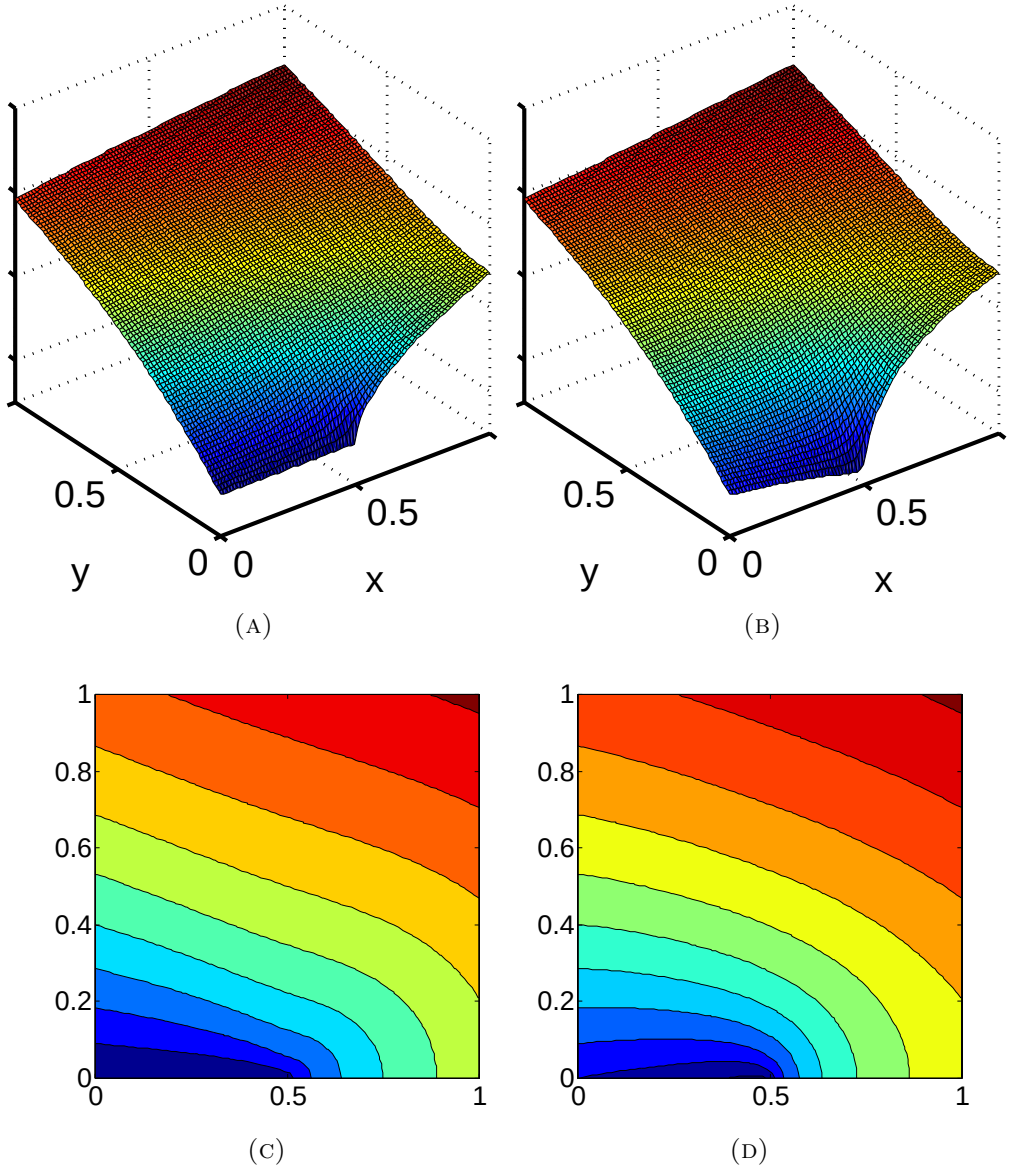

FIGURE 2.5: Local displacement field u_x (a, c). Non-local displacement field $\widetilde{u}_x$ with combined boundary conditions (b, d)

On the opposite, with alternative models, the maximum of the non-local equivalent strain appears at the crack tip, so damage correctly initiates at the crack tip.

It is worth noting that the qualitative behaviour is essentially the same for all meshes used, and for all formulations of equivalent strain (von Mises, modified von Mises and simplified Mazars). This is also true for plane stress and plane strain hypotheses, and also does not depend on the values of Poisson ratio or elasticity modulus.

This means that the second goal in this chapter has been achieved: smoothed displacement models predict correct damage initiation. This is a very important fact, as one of

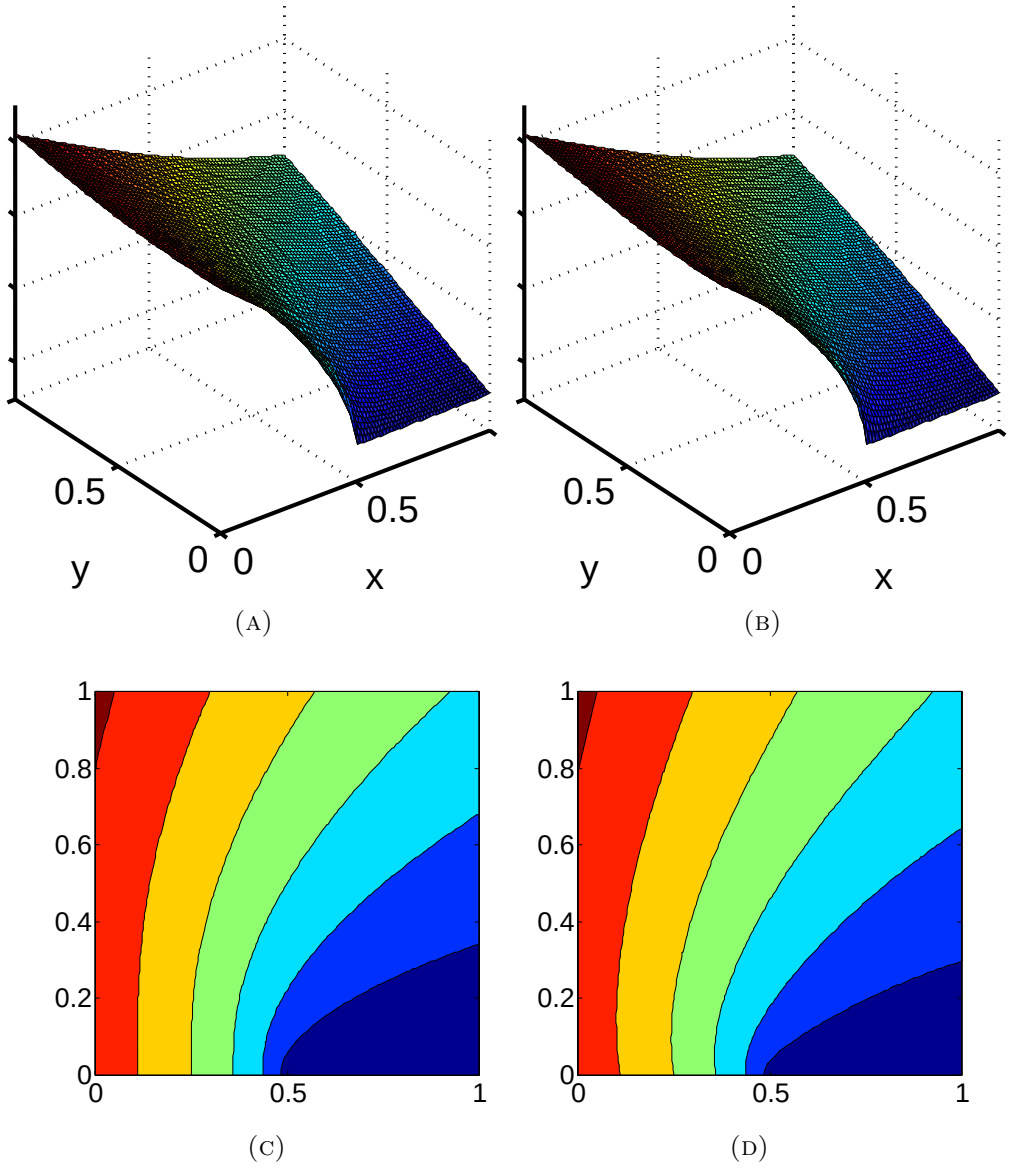

FIGURE 2.6: Local displacement field u_y (a, c). Non-local displacement field $\widetilde{u}_y$ with combined boundary conditions (b, d)

the principal problems with standard non-local models does not exist with the regularisation of displacements approach, and no additional actions are required.

2.5 Singularities

As we spoke in 2.2.2 the treatment of singularities is an interesting matter in this thesis, and that will be covered in this section.

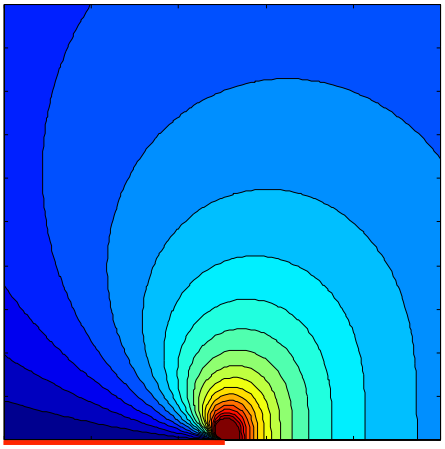

Local e

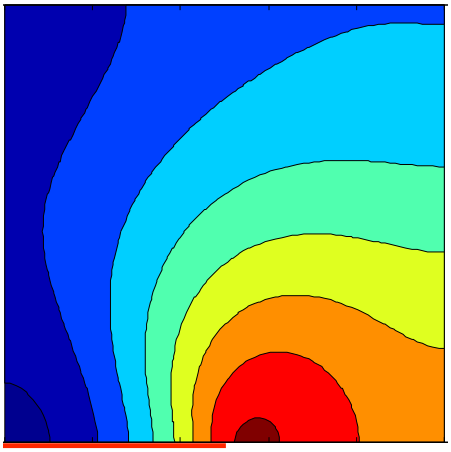

Non-local $\widetilde{e}$ (Standard model)

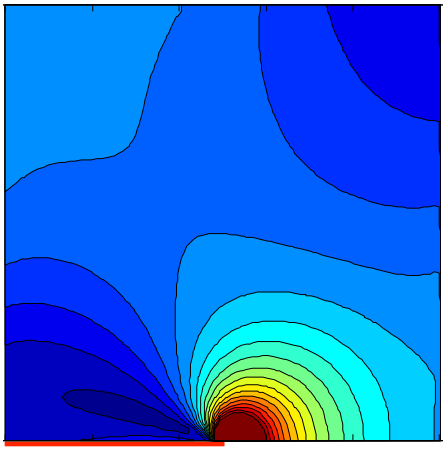

Non-local $\widetilde{e}$ (Alternative model)

FIGURE 2.7: Equivalent strain profiles

Singularities can be dangerous, and might need to get special attention when writing code (e.g. restricting the number of elements per row to an even number). Needless to say, in an ideal scenario, no singularities exist. As a reminder, in equation (2.5) we saw that local strains had a singularity due to the factor $\frac{1}{\sqrt{r}}$. Let us see what happens with the two models analysed.

In the following experiments carried out the characteristic length is $l = 0.2mm$ and the Poisson's ratio is $\nu = 0$. Different curves are plotted, which belong to different finite element meshes of 5×5, 21×21, 81×81 and 161×161 elements. Figure 2.8 represent the non-local equivalent strain at the symmetry axis.

Figure 2.8 shows that non-local equivalent strain converges to a curve for standard models. Incorrect damage initiation away from crack tip can also be appreciated. This means that standard models remove the singularities at the crack tip, but they are not able to predict the position where damage starts.

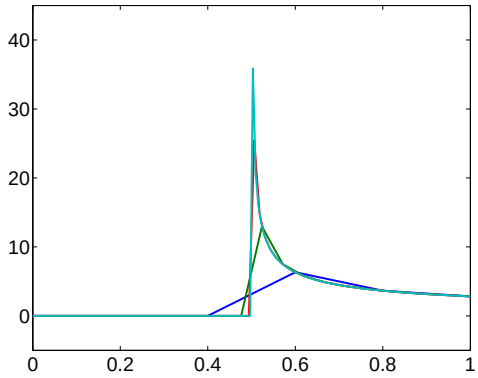

(A) Local equivalent strain e

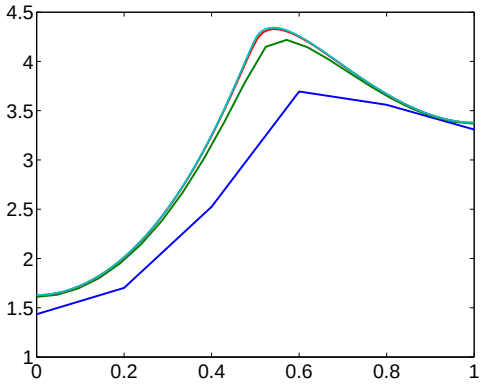

(B) Non-local equivalent strain $\tilde{e}$ (Standard model)

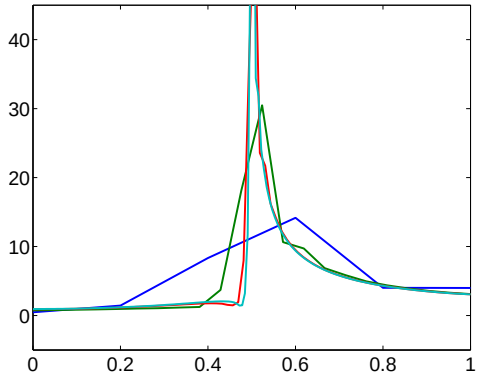

(C) Non-local equivalent strain $\tilde{e}$ (Alternative model)

FIGURE 2.8: Equivalent strain at the middle of the specimen

As for alternative models, figure 2.8 shows that the more refined the mesh is, the higher the non-local equivalent strain becomes. This is because, in denser meshes, the nodes next to the crack tip are closer to the singularity, so the strain becomes bigger. This indicates the presence of a singularity in the non-local equivalent strain generated by alternative models. Correct damage initiation at the crack tip can also be appreciated.

We will now proceed to exploit one of the advantages of smoothed displacement models. In alternative models, not only the non-local equivalent strain is calculated, non-local strains and non-local displacements are calculated as well. This way, the original source of any phenomenon we want to observe (in this case the singularities) can be found. So, recovering the fact that, on smoothed displacement models, non-local equivalent strain depends on the non-local strain tensor, these components have also been analysed.

In regards to the strains ε_{xx}, ε_{yy} and ε_{xy} we can observe in figure 2.9 that they maintain an asymptotic behaviour at the crack tip. So, singularities in the strain components are not removed.

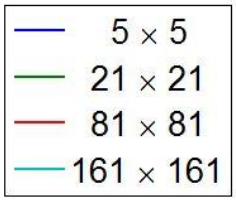

(A) Legend

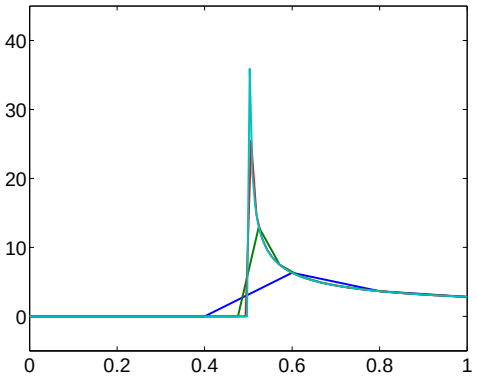

(B) Local ε_{xx}

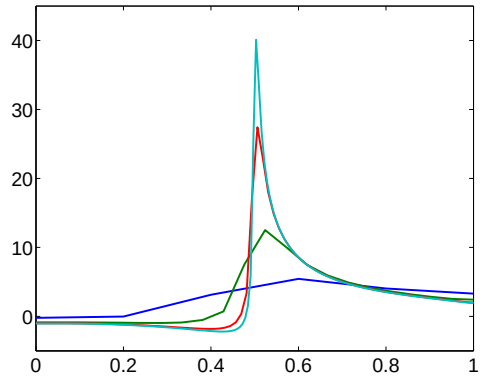

(C) Non-local ε_{xx}

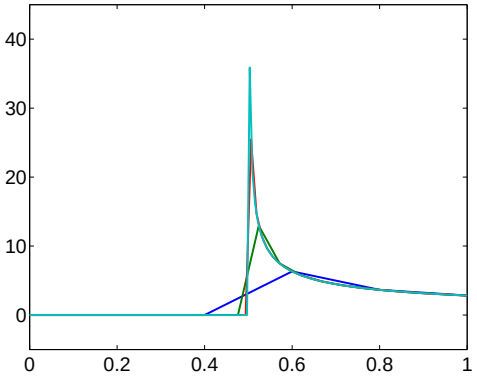

(D) Local ε_{yy}

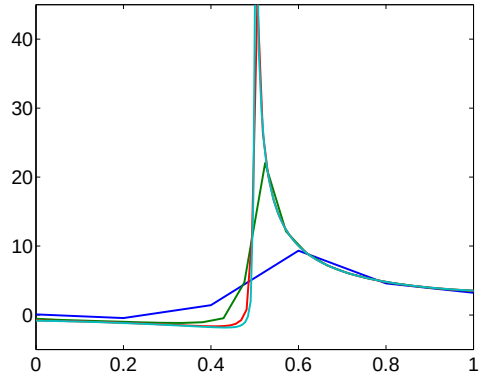

(E) Non-local ε_{yy}

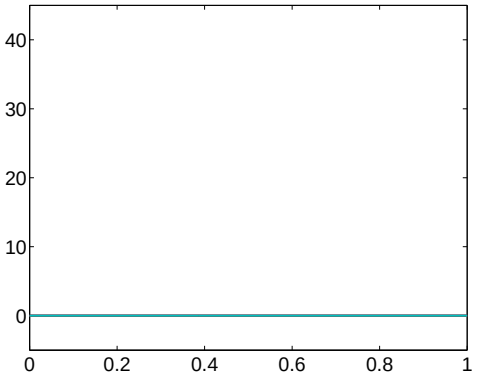

(F) Local ε_{xy}

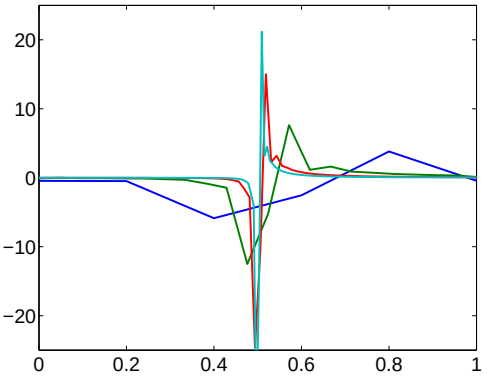

(G) Non-local ε_{xy}

FIGURE 2.9: Strain tensor components at the middle of the specimen

It is worth noting that the qualitative behaviour is essentially the same for plane stress and plane strain hypotheses, and also does not depend on the values of Poisson ratio or Young's modulus.

The plots in regards to ε_{xy} are harder to understand, but much more interesting. On the one hand, the non-local plot shows that non-local $\widetilde{\varepsilon_{xy}}$ has an asymptote at the crack tip too.

On the other hand, the local plot shows a constant zero value for ε_{xy}. This is not true, ε_{xy} is not zero among the symmetry axis, as can be deduced from equation (2.5). The reason the local ε_{xy} plot at figure 2.9 is wrong is because the asymptote at the crack tip is very pronounced. Because the size of the singularity is much smaller than the elements from the mesh, ε_{xy} is computed at the points before and after the singularity.

The behaviour in regards to singularities can be summed up as:

1. **Standard models**.
   If singularities exist at the local equivalent strain field $\tilde{e}$, they are removed.
2. **Alternative models**.
   If singularities exist at the local equivalent strain field $\tilde{e}$ or at the local strain tensor, their non-local counterparts do not remove the asymptotic behaviour.

This was already known to happen when studying gradient elasticity [11]. It is important to note that the goal in this chapter has already been achieved, and it was to demonstrate that alternative models lead to correct damage initiation at the crack tip. The presence of singularities has no disruptive effect in damage initiation, and, as we will discuss during next chapter, it is also harmless in regards the propagation of damage.

2.6 Concluding remarks

Non-local models allow to overcome the classical problems of local models, such as the inability to capture size effects and pathological mesh dependence. There are two different formulations for non-local models: gradient and integral. In this thesis, we focus on the gradient one, because it is easier to implement on boundaries.

Standard non-local models are based on the regularisation of the equivalent strain variable. These models incorrectly predict damage initiation away from crack tip in mode I problems [1]. In the presence of a predefined notch, the maximum non-local equivalent strain is inaccurately predicted, due to the singularities at the strain fields, which become infinitely large as the distance r from the crack tip tends to 0.

Alternative models, based on the regularisation of the displacement field have been presented. Since there is little research about alternative models, a discussion about boundary conditions was needed first. Combined boundary conditions (a mixture of Dirichlet and non-homogeneus Neumann) yielded best results.

The main objective during this chapter was to see if alternative models could correctly predict the maximum non-local equivalent strain at the crack tip. This goal has been achieved, and it has been demonstrated that alternative models predict correct damage initiation at the crack tip.

It was also interesting to see how standard and alternative models internally handled singularities. During the regularisation of the equivalent strain e standard models remove singularities, whereas alternative models conserve them. However, the presence of these singularities does not have negative repercussions on the characterisation of damage initiation.

2.7 Future work

Correct damage initiation has been proven with alternative models. The problem solved consisted on a specimen with a pre-existed crack under mode I failure.

There are other situations in which standard models fail to predict correct damage initiation. Beginning of damage away from the crack tip was also observed in presence of cracks or notches modelled as strongly non-convex entities with non-zero volume, without singularities [1].

Further research is required to confirm the goodness of alternative models when solving this kind of problems.

Chapter 3

Damage propagation

3.1 Introduction

During the previous chapter we have analysed how standard and alternative models handle damage initiation. Alternative models have been proven to be better in that regard, because they were able to predict correct damage initiation. The objective of this chapter is to demonstrate that alternative models also predict correct damage propagation.

Proper failure characterisation relies on proper damage initiation, so this is the reason the damage initiation analysis had to be done before the damage propagation one. Once damage has started, it propagates in a band, until the specimen collapses. In this chapter, damage propagation will be discussed.

The use of standard models to study damage propagation is not a new matter, and several test have already been done prior to this thesis. One of its uses, is to solve shear band problems. Experimental tests show that shear bands are characterised by their stationary nature in the sense that their position is determined after their formation [12]. But in the numerical results the shear band migrated from its original position, thus leading to incorrect damage propagation [1].

As standard models have been deeply discussed in the past, we will focus on damage propagation with alternative models. The goals in this chapter are:

1. **To study the evolution of the shear band during damage propagation**. Standard models wrongly predict a migration of the shear band during damage propagation processes. We will analyse how the damage band evolves when using

alternative models, and see if these models can lead to correct damage propagation, without migration of the shear band.

2. **To study the force-displacement curves during damage propagation**. Force-displacement curves are a fast and easy way to understand some of the phenomena taking place during the propagation of damage. They are related to the energy of deformation and they are a direct way to measure the ductility of a specimen. For this reason, the force-displacement curves generated by alternative models need to be addressed.

3. **To study the effect of different numerical and mechanical parameters**. Damage propagation is a more complex problem than damage initiation. In damage initiation only one state (the one which causes damage initiation) needs to be addressed, but in damage propagation all intermediate phases until collapse are interesting. For this reason, we expect that the numerical and mechanical parameters will play an important role in the propagation of the damage bands.

3.2 Description of the tests

3.2.1 Geometry

To illustrate the problem, a specimen under biaxial compression is used, as shown in figure 3.1. The reason why this case has been chosen is because this is the case in which standard gradient models failed to predict correct damage propagation [1]. The length of the specimen is $h = 60$ mm.

3.2.2 Analytical considerations

Because this problem is more complex than damage initiation, no analytical expression for displacements and strains can be found. This time the model consists of a system of two groups of differential equations: the regularisation equation (1.13) and the continuum mechanics equations.

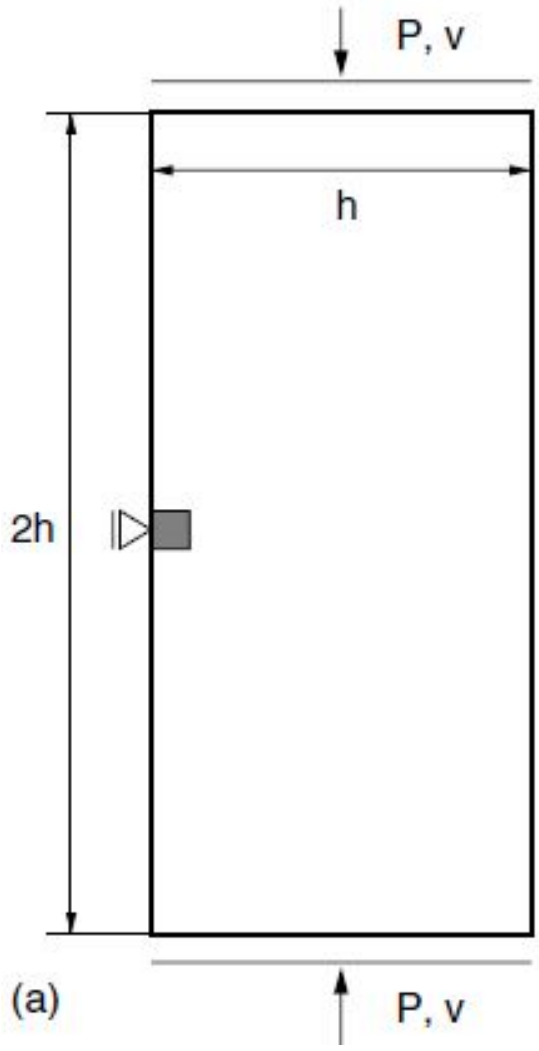

FIGURE 3.1: Geometry and loads of the specimen, from [1]

3.2.3 Material considerations

Different mathematical expressions have been used to define the softening law of the materials [3]. We will focus on the exponential law (3.1) because it is the most used, and suits the behaviour of most materials. We will also use the bilinear softening law (3.5) because of its simplicity.

For the next steps, we will consider homogeneity and isotropy of the materials, which let us write the next scalar equations. There are three reasons to do that:

1. These hypotheses are commonly taken in damage mechanics.
2. The same considerations were taken in [1].
3. This let us draw stress-strain curves, which would be impossible to do for stress and strain tensors.

Exponential softening law [13]:

$$D(\kappa) = \begin{cases} 0 & \text{if } \kappa \leq \kappa_i \\ 1 - \frac{\kappa_i}{\kappa}\Big[1 - \alpha + \alpha \exp\big(-\beta(\kappa - \kappa_i)\big)\Big] & \text{if } \kappa \geq \kappa_i \end{cases} \tag{3.1}$$

α and β are parameters that define the shape of the law and κ_i is the damage initiation strain.

By replacing (3.1) in (1.1) the stress-strain curve for the exponential damage law is obtained

$$\sigma(\varepsilon) = \begin{cases} E\varepsilon & \text{if } \kappa \leq \kappa_i \\ E\frac{\kappa_i}{\kappa}\Big[1 - \alpha + \alpha \exp\big(-\beta(\kappa - \kappa_i)\big)\Big]\varepsilon & \text{if } \kappa \geq \kappa_i \end{cases} \tag{3.2}$$

The post-peak slope of the softening branch is

$$\frac{d\sigma}{de}(\kappa_i) = -\beta E \kappa_i \tag{3.3}$$

whereas the residual stress for large strains is

$$\lim_{\boldsymbol{\varepsilon} \to \infty} \sigma(\boldsymbol{\varepsilon}) = (1 - \alpha) E \kappa_i \tag{3.4}$$

Bilinear softening law:

$$D(\kappa) = \begin{cases} 0 & \text{if } \kappa \leq \kappa_i \\ \frac{\kappa_u(\kappa - \kappa_i)}{\kappa(\kappa_u - \kappa_i)} & \text{if } \kappa_i \leq \kappa \leq \kappa_u \\ 1 & \text{if } \kappa \geq \kappa_u \end{cases} \tag{3.5}$$

where κ_u is the ultimate strain.

By replacing (3.5) in (1.1) the stress-strain curve for the bilinear damage law is obtained:

$$\sigma(\varepsilon) = \begin{cases} E\varepsilon & \text{if } \kappa \leq \kappa_i \\ E\frac{\kappa_i(\kappa_u - \kappa)}{\kappa(\kappa_u - \kappa_i)}\varepsilon & \text{if } \kappa_i \leq \kappa \leq \kappa_u \\ 0 & \text{if } \kappa \geq \kappa_u \end{cases} \tag{3.6}$$

The softening branch of the stress-strain curve has a constant slope $-\beta E \kappa_i$ with

$$\beta = \frac{1}{\kappa_u - \kappa_i} \tag{3.7}$$

Visual representations of the exponential and bilinear softening laws can be seen in figures 3.2a and 3.2b.

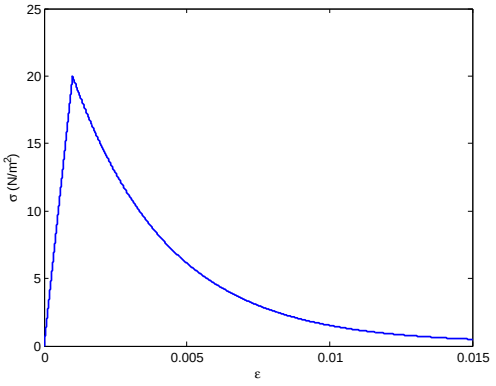

(A) Exponential softening law

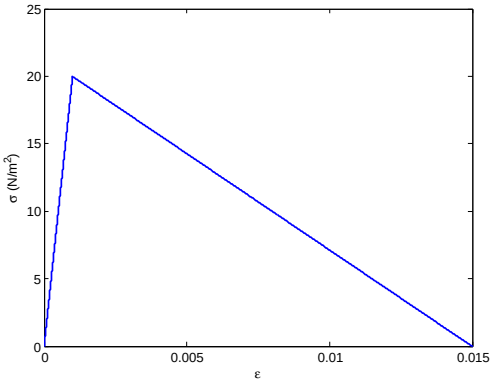

(B) Bilinear softening law

FIGURE 3.2: Example of stress-strain curves

3.2.4 Numerical considerations

In numerical simulations of quasi-static shear band formation under compressive loading, shear bands are usually triggered by an imperfection. This imperfection has been placed on the left bottom corner for the specimen, in order to observe a clearer damage band. Its size is $h/10$.

In the numerical simulations only the upper part of the specimen has been discretised due to symmetry, and the load has been applied via imposed displacements. The numerical techniques used to solve the equations are the Finite Element Method and the Newton-Raphson algorithm, with arc length control.

Because the geometry of the specimen is also a rectangle, the meshes used are the same that were used in the previous chapter, shown in figure 2.3.

3.3 Influence of the characteristic length ℓ

Throughout the following sections in this chapter it will be demonstrated that in damage propagation the choice of the physical parameters causes qualitative changes on alternative models predictions, unlike what happens in damage initiation. In this specific section we will study which is the effect of the characteristic length ℓ alone, keeping all other parameters constant.

All the tests in this section have the following material parameters, which are the same as in [1]:

Young Modulus $E = 20\ 000$ MPa
Poisson's ratio $\nu = 0.2$
Von Mises equivalent strain (equation (1.8))
Parameters of the exponential softening law (equation (3.1)):
$\kappa_i = 0.0001$
$\alpha = 0.99$
$\beta = 300$

As for the numerical parameters, the imperfection is the one described in section 3.2.1 and the meshes used are 100 by 100 elements, to guarantee enough resolution of the shear band. The characteristic length ℓ varies amongst the different tests.

Figure 3.3 shows the evolution of the shear band with $\ell = 1$ mm. In figure 3.3a it can be observed that damage starts at the imperfection, as one could have expected. The area where the imperfection is located keeps getting damaged, and later on the shear band is formed, as shown in figure 3.3b. By the end of the test, in figure 3.3c, the damage band is displaced towards the right, and almost half the specimen is damaged.

Experimental data have shown that once a shear band is created, it is stationary. So, the results shown in figure 3.3 are a big distortion of the reality and unacceptable.

In order to understand the problem, more experiments have been carried out, this time with a smaller characteristic length of ℓ=0.2 mm (five times smaller).

Figure 3.4 shows the shear band evolution of the same experiment with ℓ=0.2 mm. Damage starts at the imperfection, like in the previous example. The area where the imperfection is located keeps getting damaged, and later on the shear band is formed, as shown in 3.4b. But, by the end of the test, the width of the shear band remains unchanged (figure 3.4c).

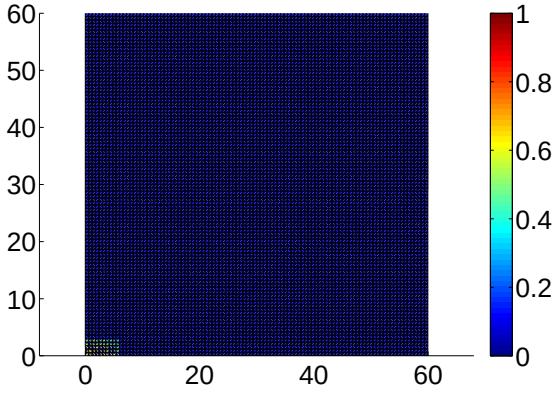

(A) Beginning of damage

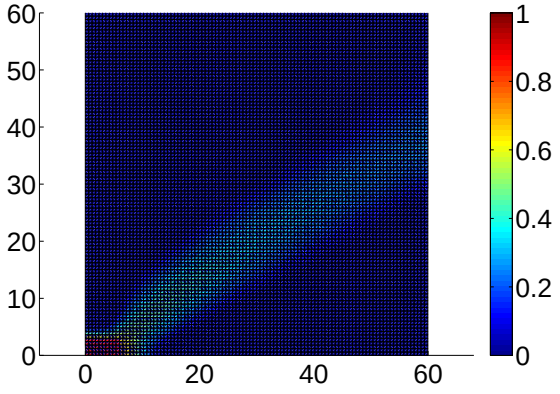

(B) Shear band formation

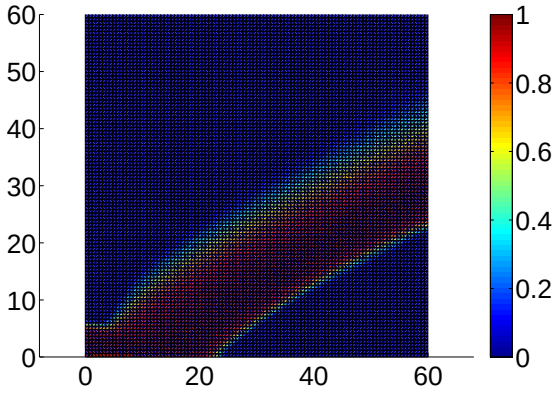

(C) Damaged specimen

FIGURE 3.3: Damage evolution. Plots of the damage field with ℓ=1 mm

On the basis of the previous representations, it seems clear that the characteristic length plays an important role when studying damage propagation. At this stage, we make an hypothesis: the larger ℓ, the larger the shear band width.

The results of a third set of tests corresponding to a length ℓ=0.6 mm are shown. The idea is to find an intermediate scenario between a varying width of the shear band (ℓ=1 mm) and a constant shear band (ℓ=0.2 mm), so the previous hypothesis can be confirmed.

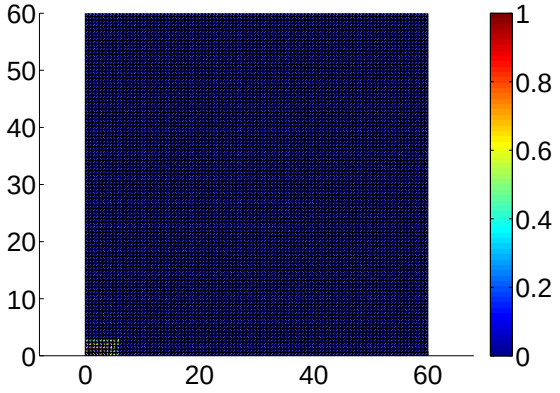

(A) Beginning of damage

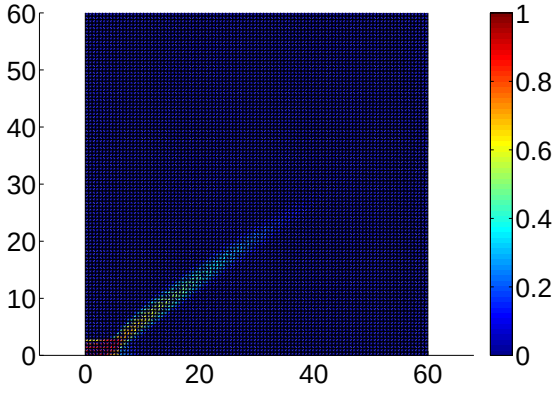

(B) Shear band formation

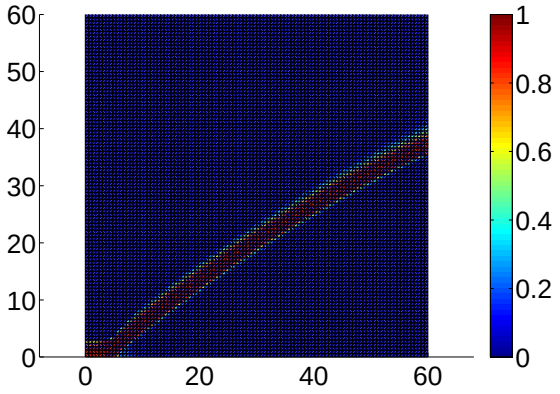

(C) Damaged specimen

FIGURE 3.4: Damage evolution. Plots of the damage field with ℓ=0.2 mm

Figure 3.5 shows the shear band evolution of the experiment with $\ell = 0.6$ mm, and it can be observed that the qualitative behaviour is the same one than with ℓ=1 mm. The damage starts at the imperfection, the shear band is formed and then expands to the right. But the width of the shear band is smaller than the one with ℓ=1 mm.

This last test let us confirm our previous hypothesis. For small characteristic length the size of the shear band is stationary, whereas when ℓ is high, there is a migration of the

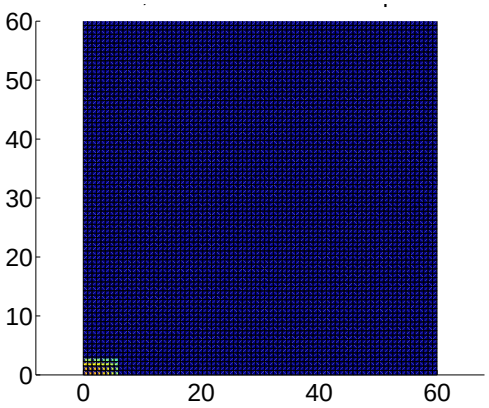

(A) Beginning of damage

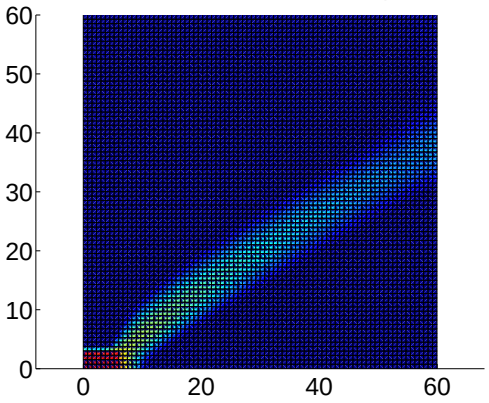

(B) Shear band formation

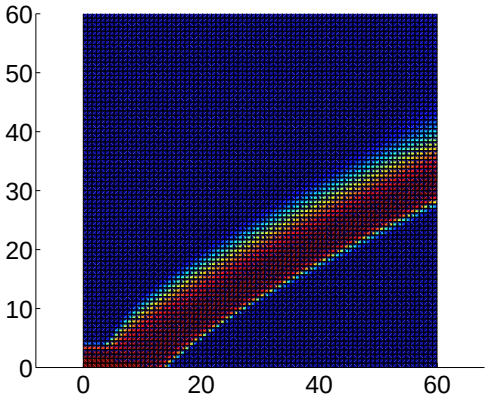

(C) Damaged specimen

FIGURE 3.5: Damage evolution. Plots of the damage field with ℓ=0.6 mm

shear band. And the higher the characteristic length, the faster the migration, and the larger the shear band.

The previous results can be interpreted as a diffusion-reaction problem. The reaction term comes from imposing displacements at the top and the diffusion term comes from the regularisation of the displacement field. Indeed, the regularisation is not anything else than smoothing the displacements, so it is logical to see it as diffusion. According

to this interpretation, higher ℓ leading to higher smoothing, leading to large bandwidth (higher diffusion) is the logical consequence.

One important thing to mention is that in [1] the tests were carried out with ℓ=1 mm and ℓ=2 mm. We have seen that, for such high values of ℓ, both alternative and standard models cause a migration of the shear band. Because of a narrow choice of ℓ in the tests from [1], there is a chance that the blame of the shear band migration was put on the model (standard models) instead of the true culprit (diffusion dominating the problems). Despite this last comment, it is important to point out that the characteristic length used for alternative models is not necessarily the same that should be used for standard models, as they are related to different equations ((1.6) and (1.13)).

When analysing damage propagation, damage profiles are not the only interesting thing to look at. Force-displacements curves are also key to understand the behaviour of a specimen under certain loads.

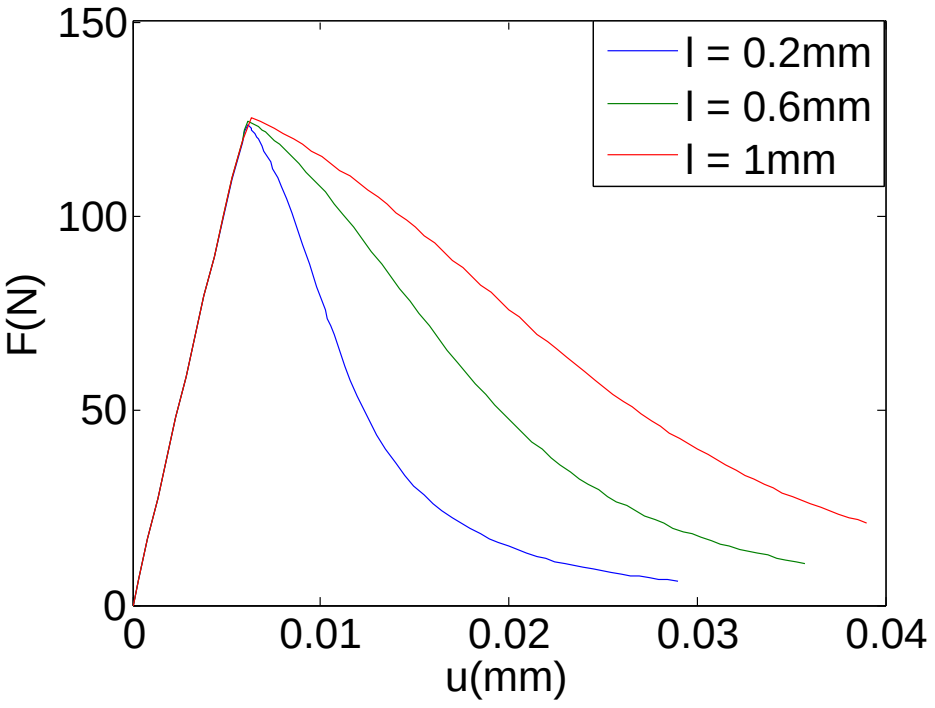

FIGURE 3.6: Force-displacement curves for different values of ℓ

Figure 3.6 shows the force-displacement curves of the previous tests. We observe that the curves with smaller ℓ are below the ones with higher ℓ. This is expected, as the area below the force-displacement curve is, by definition, the dissipated energy during the deformation. So the tests with larger damage band also have higher energy of deformation.

3.4 Influence of the softening law

In the previous section we have concluded that using a correct characteristic length is vital to ensure correct damage propagation. There is another variable that has the potential to change the qualitative behaviour of the damage propagation: the shape of the softening law.

As seen in equation (3.1) the exponential law has 2 parameters: α and β. We will focus on β, the parameter that defines the post-peak slope of the softening branch of the damage law (3.3). The physical meaning of β is related to the material resistance during damage. A high β means the specimen will lose most of its stiffness even if just damaged a little, whereas a small β means the specimen will be more resistant to damage. On the other hand, α is related to the residual force after the specimen has been fully damaged (3.4), which is not interesting for us at this time.

The reasons why it is important to analyse the effect of β are:

1. **To check that model works for different materials.**
   Previously we have studied the effect of ℓ in alternative models. ℓ is a material parameter that has to be adjusted to correctly predict propagation of damage that matches the experimental tests.

   β is a material parameter from the model too, but it is much more tied to the composition and internal structure of the material. Different tests have been carried out to ensure that alternative models can predict correct damage propagation independently of the physical properties of the material used, as long as it is a material subject to softening.

2. **To see if the parameters need to be changed**.
   In the previous section we affirmed that the characteristic length ℓ needs to be small enough to ensure correct propagation of the shear band. But defining what value of ℓ is small enough is not a trivial matter, because the correct choice of ℓ depends on the rest of the parameters of the test. We will discuss if problems with different β need to be solved with different ℓ.

The second point is quite interesting. Let us go back to the diffusion-reaction interpretation mentioned in section 3.3 and reword it a little.

When ℓ=1 mm (figure 3.3) and ℓ=0.6 mm (figure 3.5) a big part of the specimen was damaged. So, in these cases the diffusion dominated the problem. The reaction term is related to the fact that displacements are imposed at the top of the specimen. Changes

in β have a strong effect in the differential equations that describe the mechanical behaviour. If β were high enough, this could lead to the reaction term to be stronger than the diffusion one, thus not needing a small characteristic length to ensure correct damage propagation.

As a first step, the same approach that was used to study the effect of ℓ has been taken. That is, to observe the changes with different β while keeping all other parameters constant.

Young Modulus $E = 20\ 000$ MPa
Poisson's ratio $\nu = 0.2$
Von Mises equivalent strain (equation (1.8))
$\ell = 0.3$ mm
$k_i = 0.0001$
$\alpha = 0.99$

In the numerical simulations carried out, convergence of the Newton-Raphson algorithm has been very difficult for high values of β. Because of that, meshes with less density had to be used. So, in order to provide fair comparisons between all the values of β, all the meshes used have 40×40 elements.

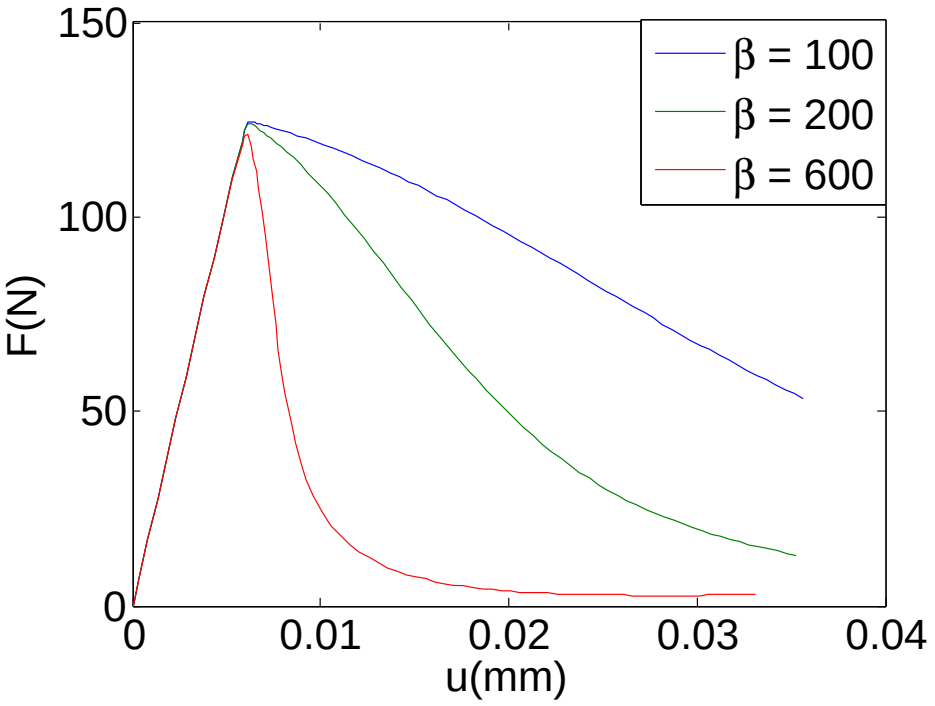

FIGURE 3.7: Force-displacement curves for different values of β

Figure 3.7 shows the force displacement curves for different values of β. As expected, smaller values of β define ductile materials, with higher energy of deformation and slower decay of the softening law.

Next we focus on damage profiles. The images of the profiles in the first states of damage are not shown, because the shape of the softening law had little effect on them. In figure 3.8 the comparison of the shear band width between $\beta = 100$ and $\beta = 200$ is made. It can be observed that the test with smaller β experiments a larger migration of the shear band.

The previous results mean that the width of the shear band depends on the speed of the damaging process: the more ductile a material is, the slower it gets damaged and the larger is the shear band.

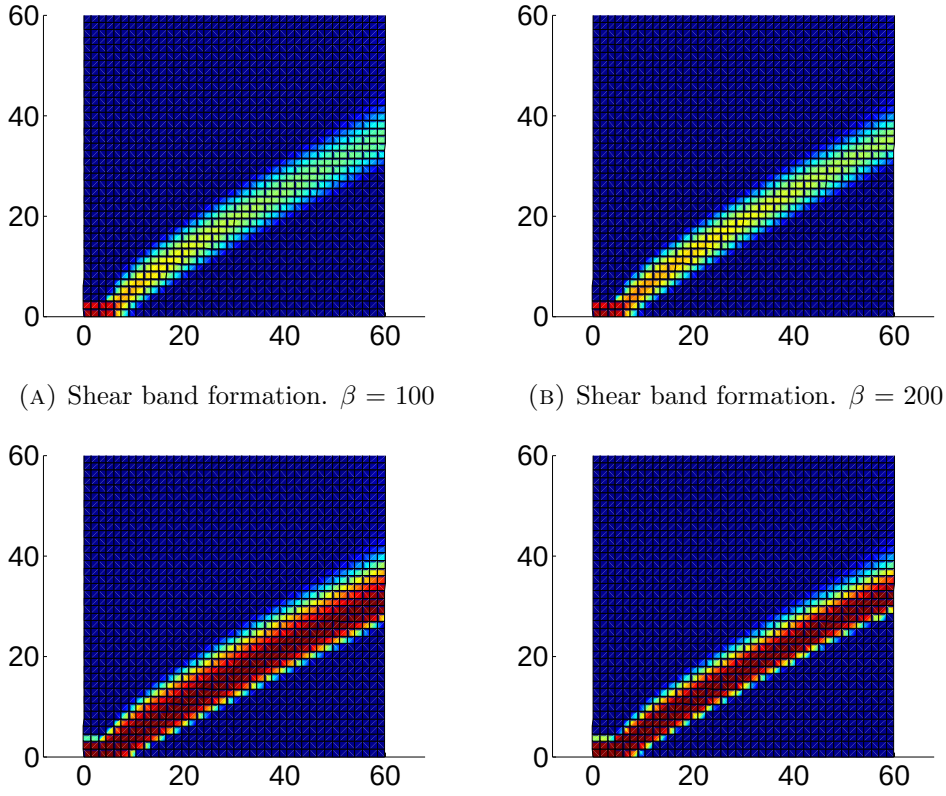

(A) Shear band formation. $\beta = 100$

(B) Shear band formation. $\beta = 200$

(C) Damaged specimen. $\beta = 100$

(D) Damaged specimen. $\beta = 200$

FIGURE 3.8: Damage evolution. Comparison with different values of β

3.5 Combined effects of ℓ and β

In the previous section it has been demonstrated that, when using alternative models, the shape of the softening law can change the width of the shear band. But it is necessary

to analyse how the parameters β and ℓ interact in order to find a characteristic length ℓ that leads to correct damage propagation (with no migration of the shear band).

Figure 3.9 shows the force-displacement curves for different combinations of ℓ and β. Specifically, it can be seen that there are three pairs of tests, and each pair has a test with $\ell = 0.3$ mm and another with $\ell = 0.6$ mm. What this figure shows is shocking at first sight: by a smart choice of ℓ, tests with different β can have very similar force-displacement curves.

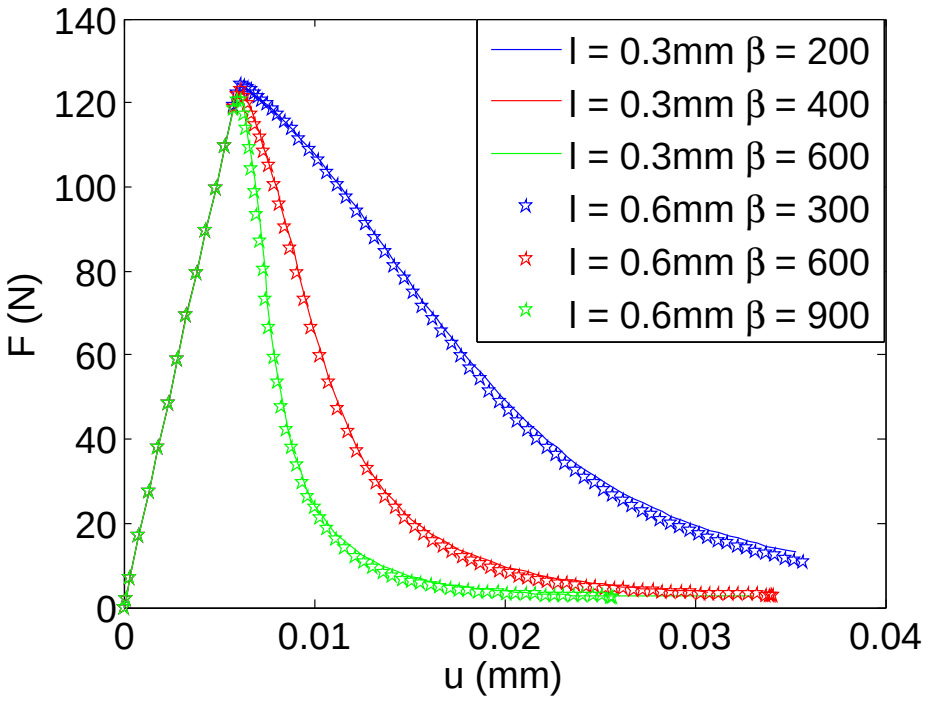

FIGURE 3.9: Force-displacement curves for different values of β and ℓ. Exponential softening law

Besides that, the origin of the curves is very different in both cases. The previous curves come from a sum through all the specimen: the parts of the specimen that are damaged highly contribute to the curve, whereas the undamaged parts have no contribution. On the one hand, decreasing β causes that each damaged part of the specimen requires more energy of deformation, thus globally increasing the total energy required.
On the other hand, increasing the characteristic length ℓ increases the width of the shear band. Because the damaged area is bigger, the total energy of deformation also becomes bigger.

Figure 3.9 has shown equivalences between $\ell = 0.3$ mm and ℓ=0.6 mm, but the same happens for other values. So, for any given pair of reference values (ℓ_0, β_0), there is another pair $(\ell,\ \beta) = (a\ell_0,\ b\beta_0)$ such that both have the same ductility, being a and b

two scalars. The relation between a and b has been found experimentally, as a correlation of the different numerical test carried out:

$$b = a^{0.58} \tag{3.8}$$

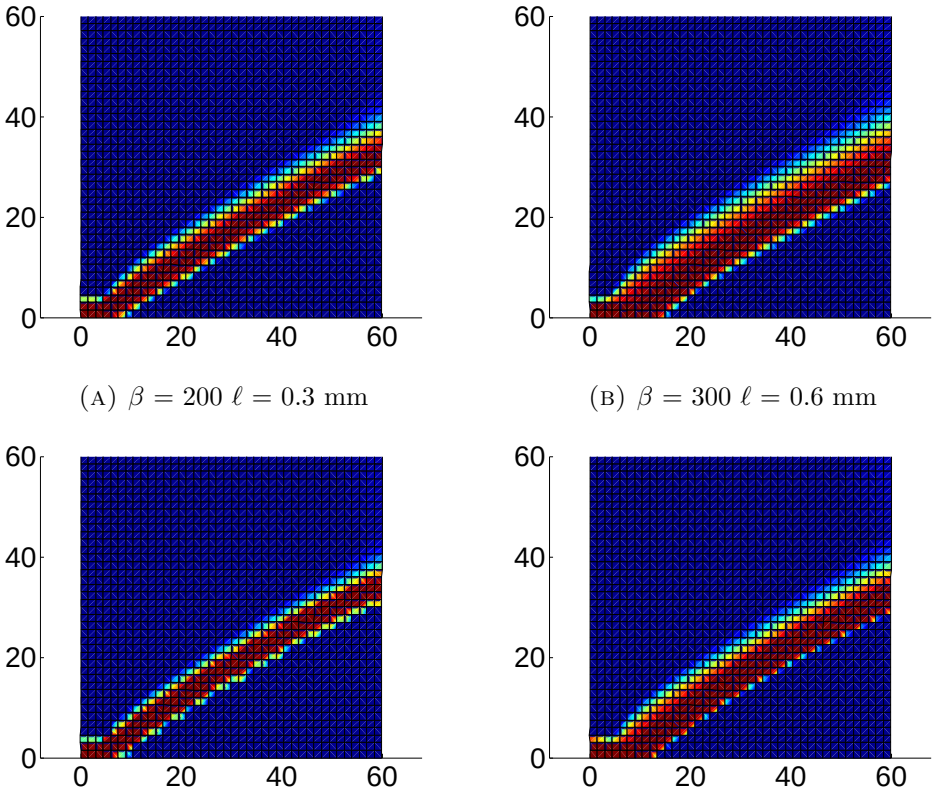

(A) $\beta = 200$ $\ell = 0.3$ mm

(B) $\beta = 300$ $\ell = 0.6$ mm

(C) $\beta = 400$ $\ell = 0.3$ mm

(D) specimen. $\beta = 600$ $\ell = 0.6$ mm

FIGURE 3.10: Damaged specimen. Comparison with different values of β and ℓ

The results from damage profiles are also very interesting. Figure 3.10 shows the damaged specimen in the same pairs of test that were used in figure 3.9. As it was said in sections 3.3 and 3.4, increasing the characteristic length and decreasing the post peak slope of the softening law causes a migration of the shear band towards the right. But, while both ℓ and β have an effect on the width of the shear band, ℓ has a stronger effect.

We have been talking about how the shape of the softening law entwines with the characteristic length, but up until now all test carried out followed an exponential softening law. In order to generalise the previous conclusions, a bilinear softening law (equation (3.5)) is considered.

This time, the parameter we have chosen to control the softening law is κ_u, and we keep κ_i constant.

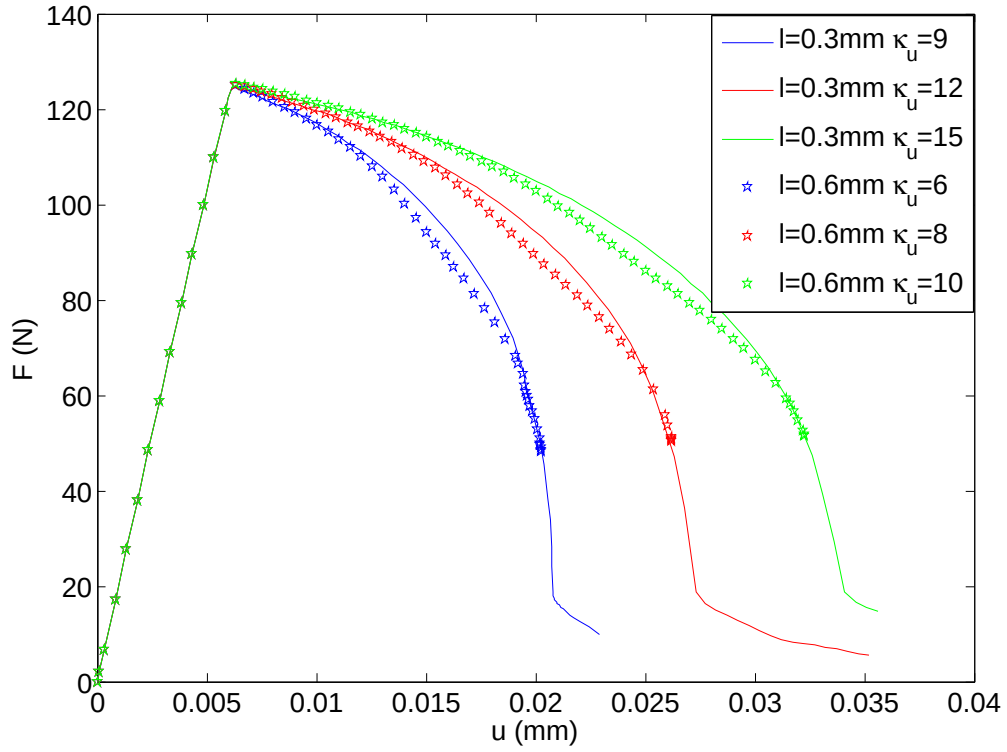

FIGURE 3.11: Force-displacement curves for different values of β and ℓ. Bilinear softening law

Following the same methodology done with the exponential softening law, different pair of values of κ_u and ℓ are compared. Figure 3.11 shows that similar load-displacements curves can be obtained by carefully choosing the values of κ_u and ℓ.

Although the fitting is not as good as with the exponential case, a similar relation to the equation (3.8) can be found for the bilinear softening law. For any given pair of reference values (ℓ_0, κ_0), there is another pair $(\ell,\ \kappa) = (a\ell_0,\ b\kappa_0)$ such that both have the same ductility, being a and b two scalars. This relation is

$$b = a^{\frac{1}{0.58}} \tag{3.9}$$

We can rewrite equation (3.9) in terms of post-peak slope of the bilinear law (equation (3.7)).

Consider reference values of the characteristic length ℓ_0 and the post-peak slope β_0. The same ductility can be obtained for $\ell = a\ell_0$ and $\beta = b\beta_0$, with

$$b = a^{0.58} \tag{3.10}$$

3.6 Analytical interpretation

Previous results and conclusions came from numerical simulations. In this section we will develop some analytical expressions that will help to understand and complement the experimental results from numerical tests.

Because getting analytical expressions for complex three-dimensional problems is out of reach, we will solve a one-dimensional problem.

3.6.1 Hypotheses and simplifications

The one-dimensional governing equations are:

Equilibrium equation

$$0 = \sigma'(\varepsilon, \tilde{\varepsilon}) = \frac{\partial \sigma}{\partial \varepsilon} u'' + \frac{\partial \sigma}{\partial \tilde{\varepsilon}} \tilde{u}'' \tag{3.11}$$

Regularisation equation:

$$u = \tilde{u} - \ell^2 \tilde{u}'' \tag{3.12}$$

The tension is uni-axial with no loading-unloading cycles, so $\kappa \equiv \tilde{\varepsilon}$.

We consider a reference state, in which the displacement u_0 is linear. For a linear field u, the solution of the equation (3.12) is $\tilde{u} = u$. Thus, at the reference state $\tilde{u}_0 = u_0$ and $\varepsilon = \tilde{\varepsilon} = \varepsilon_0$.

The reference state is submitted to infinitesimal perturbations δu and $\delta \tilde{u}$. These perturbations take the shape of harmonic functions, so:

$$\delta u = A_1 \cos kx \delta \tilde{u} = A_2 \cos kx \tag{3.13}$$

where A_1,A_2 are two amplitudes and k is a finite and real wave number.

Substituting (3.13) in (3.12) leads to:

$$A_1 = A_2(1 + k^2 \ell^2 \tag{3.14}$$

And substituting (3.13) in (3.11) leads to:

$$(1 + k^2 \ell^2) \frac{\partial \sigma}{\partial \varepsilon} + \frac{\partial \sigma}{\partial \tilde{\varepsilon}} = 0 \tag{3.15}$$

with

$$\frac{\partial \sigma}{\partial \varepsilon} = \big(1 - D(\tilde{\varepsilon})\big) E \quad ; \quad \frac{\partial \sigma}{\partial \tilde{\varepsilon}} = -\frac{\partial D}{\partial \tilde{\varepsilon}} E \varepsilon \tag{3.16}$$

Replacing (3.16) in (3.15) results in

$$(1+k^2\ell^2)\big(1-D(\tilde{\varepsilon})\big)-\frac{\partial D}{\partial\tilde{\varepsilon}}\varepsilon=0 \tag{3.17}$$

3.6.2 Critical wave length

Bilinear law [14] :

$$D(\tilde{\varepsilon})=\frac{\kappa_u(\tilde{\varepsilon}-\kappa_i)}{\tilde{\varepsilon}(\kappa_u-\kappa_i)} \quad ; \quad \frac{\partial D}{\partial\tilde{\varepsilon}}=\frac{\kappa_i\kappa_u}{\tilde{\varepsilon}^2(\kappa_u-\kappa_i)} \tag{3.18}$$

Replacing (3.18) in (3.17) and evaluating at the uniform reference state ε_0 leads to

$$(1+k^2\ell^2)(\kappa_u-\varepsilon_0)-\kappa_u=0 \tag{3.19}$$

The solution of this equation is the critical wave number k_{crit} and the corresponding critical wave length λ_{crit}:

$$k_{\text{crit}}=\frac{1}{\ell}\sqrt{\frac{\varepsilon_0}{\kappa_u-\varepsilon_0}} \quad ; \quad \lambda_{\text{crit}}=\frac{2\pi}{k_{\text{crit}}}=2\pi\ell\sqrt{\frac{\kappa_u-\varepsilon_0}{\varepsilon_0}} \tag{3.20}$$

Finally, assuming that $\varepsilon_0=\kappa_i$ (i.e. localisation starts at damage initiation strain) and taking into account (3.7) yields

$$\lambda_{\text{crit}}=2\pi\ell\sqrt{\frac{\kappa_u-\kappa_i}{\kappa_i}}=C_\lambda\frac{\ell}{\sqrt{\beta}} \qquad \text{with} \qquad C_\lambda=\frac{2\pi}{\sqrt{\kappa_i}} \tag{3.21}$$

Exponential law:

$$\begin{aligned} D(\tilde{\varepsilon}) &= 1-\frac{\kappa_i}{\tilde{\varepsilon}}\Big[1-\alpha+\alpha\exp\big(-\beta(\tilde{\varepsilon}-\kappa_i)\big)\Big] \\ \frac{\partial D}{\partial\tilde{\varepsilon}} &= \frac{\kappa_i}{\tilde{\varepsilon}^2}(1-\alpha)+\Big(\frac{1}{\tilde{\varepsilon}}+\beta\Big)\frac{\kappa_i}{\tilde{\varepsilon}}\alpha\exp\big(-\beta(\tilde{\varepsilon}-\kappa_i)\big) \end{aligned} \tag{3.22}$$

Replacing (3.22) in (3.17) and evaluating at the uniform reference state $\varepsilon_0=\kappa_i$ leads to

$$(1+k^2\ell^2)-(1+\alpha\beta\kappa_i)=0 \tag{3.23}$$

The corresponding critical values are

$$k_{\text{crit}}=\frac{1}{\ell}\sqrt{\alpha\beta\kappa_i} \tag{3.24}$$

and

$$\lambda_{\text{crit}} = \frac{2\pi}{k_{\text{crit}}} = 2\pi\ell\sqrt{\frac{1}{\alpha\beta\kappa_i}} = \frac{1}{\sqrt{\alpha}} C_\lambda \frac{\ell}{\sqrt{\beta}} \tag{3.25}$$

3.6.3 Area under stress-strain curve

Consider the local stress-strain curve, with $\tilde{\varepsilon} \equiv \varepsilon$. The goal of this subsection is to compute the area under the stress-strain curve (that is, the point-wise ductility) for the various damage evolution laws.

Bilinear law:

$$\begin{aligned} A = \int_0^\infty \sigma(\varepsilon)d\varepsilon &= \int_0^{\kappa_i} \sigma(\varepsilon)d\varepsilon + \int_{\kappa_i}^{\kappa_u} \sigma(\varepsilon)d\varepsilon + \int_{\kappa_u}^\infty \sigma(\varepsilon)d\varepsilon \\ &= \frac{1}{2}E\kappa_i^2 + \frac{1}{2}E\kappa_i(\kappa_u - \kappa_i) + 0 = \frac{1}{2}E\kappa_i\kappa_u \end{aligned} \tag{3.26}$$

(Expected result: the stress-strain curve is a triangle of side κ_u and height $E\kappa_i$).

Exponential law:

The total area A is unbounded for $\alpha < 1$, because the stress tends to $(1-\alpha)E\kappa_i$, not to 0, as strain tends to infinity, see (3.4). For the range $0 < \varepsilon < \varepsilon_{\max}$ the area is

$$\begin{aligned} A = \int_0^{\varepsilon_{\max}} \sigma(\varepsilon)d\varepsilon &= \int_0^{\kappa_i} \sigma(\varepsilon)d\varepsilon + \int_{\kappa_i}^{\varepsilon_{\max}} \sigma(\varepsilon)d\varepsilon \\ &= \frac{1}{2}E\kappa_i^2 + \int_{\kappa_i}^{\varepsilon_{\max}} E\kappa_i\Big[1 - \alpha + \alpha\exp\big(-\beta(\varepsilon - \kappa_i)\big)\Big]\, d\varepsilon \\ &= \frac{1}{2}E\kappa_i^2 + E\kappa_i\Big[(1-\alpha)(\varepsilon_{\max} - \kappa_i) + \frac{1}{\beta} - \frac{\alpha}{\beta}\exp\big(-\beta(\varepsilon_{\max} - \kappa_i)\big)\Big] \\ &= E\kappa_i\left(\frac{1}{2}\kappa_i + \frac{1}{\beta} + (1-\alpha)(\varepsilon_{\max} - \kappa_i) - \frac{\alpha}{\beta}\exp\big(-\beta(\varepsilon_{\max} - \kappa_i)\big)\right) \end{aligned} \tag{3.27}$$

3.6.4 Ductility of shear band test

The goal of this subsection is to explore the influence of the characteristic length ℓ and the post-peak slope, represented by parameter β, in the ductility $\mathcal{D}$ (that is, the area under the force-displacement curve) of the shear band test. In order to do so, the following simplifying assumptions are made:

1. The area of the shear band (i.e. damaged zone) is proportional to the critical wave length λ_{crit}, see subsection 3.6.2.

2. All points within the shear band undergo full softening, so the point-wise energy dissipation is the area A under the stress-strain curve computed in subsection 3.6.3.

With these assumptions, the ductility can be expressed as

$$\mathcal{D} = c\lambda_{\text{crit}} A \tag{3.28}$$

where c is the constant of proportionality mentioned in hypothesis 1 above.

Bilinear law:
Replacing (3.21) and (3.26) in (3.28) results in

$$\mathcal{D} = cC_\lambda \frac{\ell}{\sqrt{\beta}} \frac{1}{2} E\kappa_i\kappa_u \tag{3.29}$$

If one assumes $\kappa_u >> \kappa_i$, then $\kappa_u \approx 1/\beta$ and (3.29) can be rewritten as

$$\mathcal{D} = C_{\text{linear}} \frac{\ell}{\beta^{3/2}} \qquad \text{with} \qquad C_{\text{linear}} = c\pi E\sqrt{\kappa_i} \tag{3.30}$$

Exponential law:
The estimation of ductility is less clear in this case, because the area under the stress-strain curve is infinite. However, if the strain is bounded by $\varepsilon_{\max}$ and one assumes that $1/\beta$ dominates the other summands in the right-hand-side of (3.27), then the ductility can be approximated by (3.31).

$$\mathcal{D} = C_{\text{exp}} \frac{\ell}{\beta^{3/2}} \qquad \text{with} \qquad C_{\text{exp}} = 2c\pi E\sqrt{\kappa_i} \tag{3.31}$$

Note that $C_{\text{exp}} = 2C_{\text{linear}}$: for the same post-peak slope, exponential softening is twice as ductile as linear softening, cf. (3.30) and (3.31).

3.6.5 Conclusions from the analytical problem solved

For the various damage evolution laws analysed, the ductility is estimated as

$$\mathcal{D} = C \frac{\ell}{\beta^{3/2}} \tag{3.32}$$

The larger the characteristic length, the larger the ductility: diffusion in the regularisation equation (1.13) is a source of ductility. The smaller the post-peak slope, the larger the ductility: a mild softening branch in the stress-strain curve is also a source of ductility.

Consider reference values of the characteristic length and the post-peak slope, ℓ_{ref} and β_{ref}. The same ductility can be obtained for $\ell = a\ell_{\text{ref}}$ and $\beta = b\beta_{\text{ref}}$, with

$$\frac{a}{b^{3/2}} = 1 \Longrightarrow b = a^{2/3} \tag{3.33}$$

The analytical relation from (3.33) is very similar to the ones from numerical experiments (3.8) and (3.10). This is a very good sign.
On the one hand both expressions having the same order of magnitude ensures that the numerical test were done correctly. And on the other hand, having some analytical expressions gives a better understanding of the model.

The small difference in the value of the exponent (2/3 against 0.58) is not a big concern. Mainly because the numerical problem was 2D, whereas the analytical one was 1D, and several assumptions had been done. But also because numerical adjustment to mathematical expressions is rarely perfect, higher number of test might yield more accurate correlations.

3.7 Concluding remarks

As in the previous chapter, alternative models have been proposed as an alternative to standard models. The reason to do so was the incapacity of standard models to properly describe damage propagation: as the specimen gets damaged, the shear band migrates.

So, the main objective during this chapter has been to demonstrate that alternative models accurately predict the correct size of the shear band during the damage propagation process, and also to check that they do not have other drawbacks.

The results of the research show that alternative models are capable of properly describing damage propagation, but a precise choice of the material parameters has to be done. High values of the characteristic length ℓ lead to same problems that standard models have, leading to a migration of the shear band. But small values of ℓ lead to an accurate propagation of damage. The cause of this is that, in a damage propagation problem, ℓ is a source of diffusion. Too much diffusion leads to a non-physical migration of the shear band.

In addition, the effect of ℓ is not isolated, but depends on the shape of the softening law. Ductile materials require very low values of ℓ to ensure that the shear band does not migrate during damage propagation, whereas with fragile materials these restrictions to ℓ are not so strong, and medium-low values of ℓ are enough. Although both parameters have the potential of incorrectly causing a migration of the shear band, the effect of ℓ

has been proven to be stronger than the post-peak slope of the softening lawβ. Thus, higher emphasis must be put on the choice of an adequate ℓ.

Lastly, it has been found out that the characteristic length ℓ also has impactful repercussions on the total energy of deformation of a specimen. In fact, same force-displacement curves could be obtained starting from two materials with different softening laws, by carefully choosing the appropriate ℓ. The cause of this is the fact that increasing ℓ increases size of the damaged area, so more elements are damaged, leading to higher energy required.

This influence of ℓ and β on the ductility of a specimen has been quantified. The expressions that relate both parameters have been found by adjusting the results from different numerical experiments (3.8) (3.10), and verified analytically in a one-dimensional problem (3.33).

We have identified an intrinsic problem of non-local models in shear bands' characterisation (incorrect migration of the shear band when there is too much diffusion). We also have found its cure, which was probably overlooked in [1] (a proper characterisation of the material parameters ℓ and β). We have enough traces to think that this is a feature shared among both standard and alternative models. We also believe that the study of the ductility as a function of ℓ and β can be exported to other cases, and similar conclusions can be drawn for standard or other non-local models.

3.8 Future work

This chapter has answered a lot of questions, but it has also opened many more questions and possibilities.
During this thesis, we have considered that the characteristic length ℓ is constant. But what would happen in a gradient model based on the regularisation of displacements, whose ℓ is not a constant but instead, ℓ is a function of damage?
If alternative models (gradient based) can correctly capture sharp shear bands, can their integral counterpart (non-local integral models based on the regularisation of displacements) achieve the same?
Another research topic is to check if what has been discovered about alternative models regarding damage propagation is exclusive to alternative models, or a common feature of all non-local gradient models that had been overlooked in the past.

Chapter 4

Summary and future work

Throughout this thesis two different non-local gradient enhanced models have been compared: standard models (based in smoothing the equivalent strain) and alternative models (based in smoothing the displacements).

The motivation of this work was the incapacity of standard models to accurately predict damage initiation and damage propagation [1], and alternative models were proposed as a solution to the difficulties that standard models face.

We can conclude that alternative models correctly predict damage initiation and damage propagation.

The main conclusions regarding damage initiation are:

1. Combined boundary conditions (a mixture of Dirichlet and non-homogeneus Neumann) provide a good behaviour of alternative models.
2. Alternative models correctly predict damage initiation at a crack tip, whereas standard models incorrectly predict damage initiation away from the crack tip [1].
3. Singularities are not removed by alternative models, but this has no negative effect neither in damage initiation nor in damage propagation.

The main conclusions regarding damage propagation are:

1. Alternative models can capture sharp shear bands accurately.
2. Standard models were said to cause a migration of the shear band [1], but we have found evidence that this might not be true.

3. In order to correctly predict damage propagation, the adequate choice of the material parameters is key. A high characteristic length ℓ leads to a problem dominated by diffusion and non-physical shear band migration.

4. The characteristic length ℓ and the slope of the softening law β determine the ductility of a specimen. High ℓ produces diffusion, increasing ductility, whereas high β leads to a fast damaging process, lowering the ductility. Similar conclusions can probably be drawn for other models, but further research is necessary to prove it.

5. β also affects the width of the damage band, but the influence of ℓ is significantly higher.

The results from damage initiation are very clear: alternative models lead to correct damage initiation at the crack tip, whereas standards models do not. On the opposite, the results from damage propagation are open to further discussion on a wide variety of topics, such as exploring alternative models into integral formulations, or models based on anisotropic regularisation (ℓ depending on damage, instead of being a fixed parameter). Future research could also be aimed at studying the effects of β and ℓ in standard models.

Bibliography

[1] A. Simone, H. Askes, and L.J. Sluys. Incorrect initiation and propagation of failure in non-local and gradient-enhanced media. *International Journal of Solids and Structures*, 41(2):351–363, 2004.

[2] Z.P. Bazant and M. Jirasek. Nonlocal integral formulations of plasticity and damage: Survey of progress. *Journal of Engineering Mechanics*, 128(11):1119–1149, 2002.

[3] E. Tamayo-Mas. *Continuous-discontinuous modelling for quasi-brittle failure: propagating cracks in a regularised bulk.* PhD thesis, Universitat Politecnica de Catalunya, October 2013.

[4] A. Rodríguez-Ferran, I. Morata, and A. Huerta. A new damage model based on non-local displacements. *International Journal for Numerical and Analytical Methods in Geomechanics*, 29(5):473–493, 2005.

[5] R.H. Peerlings, R. de Borst, W.A. Brekelmans, J.H. de Vree, and I. Spee. Some observations on localisation in non-local and gradient damage models. *European Journal of Mechanics A-Solids*, 15(6):937–953, 1996.

[6] J.H. de Vree, W.A. Brekelmans, and M.A. Vangils. Comparison of nonlocal approaches in continuum damage mechanic. *Computers and Structures*, 55(4):581–588, 1995.

[7] J. Mazars. A description of microscale and macroscale damage of concrete structures. *Engineering Fracture Mechanics*, 25(5-6):729–737, 1986.

[8] X. Oliver and C. Agelet. *Mecánica de medios continuos para ingenieros.* Edicions UPC, 2000.

[9] E. Tamayo-Mas and A Rodríguez-Ferran. Boundary conditions for gradient-enhanced models with smoothed displacements. *Revista Internacional de Métodos Numéricos para Cálculo y Diseño en Ingeniería*, 28(3):170–176, 2012.

[10] C.T. Sun and Z.H. Jin. *Fracture Mechanics.* Elsevier Inc., 2012.

[11] H. Askes, I. Morata, and E.C. Alfantis. Finite element analysis with staggered gradient elasticity. *Computers and Structures*, 86(11-12):1266–1279, 2008.

[12] S. Nemat-Nasser and N. Okada. Radiographic and microscopic observation of shear bands in granular materials. *Geotechnique*, 51(9):753–765, 2001.

[13] R.H. Peerlings, R. de Borst, W.A. Brekelmans, and J.H. de Vree. Gradient enhanced damage for quasi-brittle materials. *International Journal for Numerical Methods in Engineering*, 39(19):3391–3403, 1996.

[14] A. Rodríguez-Ferran, T. Bennett, H. Askes, and E. Tamayo-Mas. A general framework for softening regularisation based on gradient elasticity. *International Journal of Solids and Structures*, 48(9):1382–1394, 2012.